TIANJIN UNIVERSITY
GRADUATION PROJECT (THESIS) OF UNDERGRADUATE

Title: “Design and simulation of a 3D porous copper solar-driven evaporator"

School	**Environmental Science and Engineering**
Major	**Environmental Engineering**
Year of Enrollment	**2017**
Name	**Pierre Alexander Porras Jorge** 亚历山大
Student ID	**6317000004**
Supervisor	刘宪华

Statement of Originality

I declare that the submitted graduation project (thesis) is the result of my research work under the guidance of my supervisor. Except for the content that has been cited in the text, this graduation project (thesis) does not include any research results that have been published or written by others. Other individuals and groups who have contributed to the research work of this graduation project (thesis) have been clearly stated. The legal responsibility for this original statement of the graduation project (thesis) shall be borne by myself.

Author's signature:
Date(Y/M/D):

I declare that this graduation project (thesis) is completed by the student under my guidance, and I have reviewed the entire content of the project (thesis).

Supervisor’s signature:
Date(Y/M/D):

ABSTRACT

Solar steam generation has attracted huge research awareness about consideration owing to its high efficiency in solar energy and transformative mechanical potential. Recently, solar-driven interfacial evaporation by localization of solar-thermal energy conversion in the air/liquid interface has been suggested as a positive alternative to conventional bulk heating-based evaporation, conceivably decreasing thermal losses and progressing energy transformation effectiveness.

This graduation project proposes the development of a unique 3D copper porous solar-driven evaporation design which is composed of a transparent cover (transparent bubble wrap), a spectrally selective solar absorber, an evaporation structure (hybrid copper porous foam), a wicking material (air-laid paper) and a thermal insulation (polystyrene and EPE foam). Moreover, the design is simulated in COMSOL Multiphysics software and high solar-to-steam efficiency of 48.1%. The high steam generation efficiency is reached by localizing solar-thermal heating at the evaporation surface and controlling the water supply onto the porous evaporator by adjusting its surface wettability, which anticipates overheating of the evaporator and in this way minimizes conductive, convective, and warm radiative losses from the evaporator. The unique design of the steam outlet placed at the sidewall of the evaporator encourages the collection of produced steam; in addition, it maintains a strategic distance from potential blockage of solar radiation by the condensing steam. The high-efficiency solar-driven evaporator can be utilized in many technologically critical energy-related applications such as solar-thermal energy harvesting, electricity generation, mechanical energy harvesting, and solar- chemical fuel production.

Key words: Solar, evaporation, water, thermal, steam, energy, heat, generation, driven, interfacial, high, surface, foam, porous, and efficiency.

Contents

Chapter 1 Introduction

1.1 Research background

The Sun is a promising renewable energy source to propel the sustainable development of human society[1,2]. Sunlight can be transformed over straightforwardly into power through the photovoltaic process and heat through solar-thermal technology[3,4]. Solar-thermal innovation could be a direct way to collect sun-based energy for heating and energy capacity applications[1,2,5-7].

One implementation of solar-thermal technology, solar-driven evaporation, involves the generation of vapors at temperatures lower than the boiling temperature and the generation of steam at or above the boiling temperature[8]. As a fundamental thermal process, solar-driven evaporation plays a ubiquitous role in driving diverse applications globally[9,10], and has been utilized by people to create clean water since antiquated times[11]. It has moreover been utilized to examine numerous critical industrial operations and has been used by humans to generate clean water since ancient times[11]. It has also been used to drive many important industrial process operations, such as power generation[14] and steam sterilization[13], in modern society. The harvested thermal energy can drive many essential processes such as domestic heating,[14] seawater desalination,[11,15] sterilization,[13,16,17] distillation,[18,19] and electrical power generation[12].

To realize the high performance of the solar-thermal framework, high-efficiency steam or vapor generation at elevated temperatures[20] is the vital variable. 1 solar flux (1 kW/m^2) is insufficient to provide sufficient solar-heating density to generate hot steam due to the vaporization enthalpy of water (2.26 x 10^6 J/kg at 100 ˚C)[21]. In recent years, solar-driven interfacial evaporation, which localizes sun-powered warming at the air-water interface instead of warming up the bulk fluid, has emerged as a new form of evaporation design[8,22-24]. The difference is that interfacial evaporation systems have demonstrated significantly increased solar-to-vapor conversion efficiency and faster response due to reduced heat losses and smaller thermal masses[8,24].

Other technologies to increase solar-to-vapor efficiency to ~90%: (1) Synthesizing new solar-absorbing materials[25,26]; (2) Tailoring microstructure of the solar absorbers[27,28]; Improving thermal insulation[29,30]; (3) Capillary water supplying design[31,32]; (4) Optimizing evaporator structure[33,34].

The high-performance solar-driven interfacial evaporation has enabled: (1) High-performance steam generation[35,36]; (2) Solar desalination[32,37-40].; (3) Multifunctional clean water generation[35,36]; (4) Electricity generation[41,42] under reduced solar concentration.

Most recent research interest has been directed to vapor generation under natural 1 sun illumination conditions[43-45], without the necessity for optical concentrators, which include a significant fee to the dissipation frameworks conjointly give up the in general vitality change productivity of the framework due to the expanded heat dissipation from the hot sun-based collector surfaces. The steam generation under low solar flux, 1 sun illumination with a power density of 1 kW/m^2 is still challenging. Solar-driven interfacial evaporation has the capacity to extend the utilization of solar-thermal innovations in compact, stand-alone, and portable systems[23,24,39,49]. In consequence, this graduation project presents a unique 3D copper porous solar-driven evaporation design through a transparent bubble wrap, a spectrally selective solar absorber, a hybrid copper porous foam, air-laid paper, and a polystyrene and EPE foam. The design can generate 100 ˚C steam under 1 sun illumination with a high solar-to-steam efficiency of 48.1%. In addition, the importance of the evaporation surface, water supply control to the porous evaporator, and outlet steam will be explained in the following chapters.

1.2 Overview of solar-driven interfacial evaporation system

The development of the solar-driven interfacial evaporation system centers around the following key components:

(1) A solar absorber that can efficiently absorb and change over the sun-oriented radiation into heat whereas enabling the vapor to permeate through the front cover;

(2) A floating evaporation structure that can simultaneously maximize the evaporation rate and supply liquid to the heated region;

(3) A thermal insulator that can effectively reduce the loss of the transformed solar-thermal vitality to the bulk fluid.

1.2.1 Solar absorbers

Proficient absorption of the broad-spectrum powered radiation and its transformation into heat is the primary essential step to drive fluid evaporation. The two categories of solar-absorbing materials presented are carbon-based[24,50-52] and plasmonic-based[27,39,53,54] absorbers.

1.2.1.1 Carbon materials

Clearly, black materials are suitable for broad-band solar absorption[55]. Sun-oriented absorption in carbon-based materials includes the excitation of electrons and their consequent unwinding. The optically energized electrons are rapidly thermalized by electron-electron and electron-phonon scattering[55].

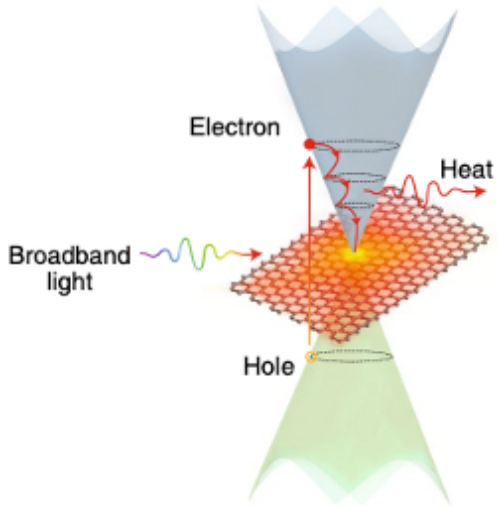

Figure 1-1 Working principles of solar-thermal conversion for graphene, a type of carbon-based solar absorber. When the incident sunlight shines onto the monolayer graphene, which is a zero-bandgap semiconductor, it excites the electrons from the valence band (green cone) to the conduction band (grey cone), and the relaxation of the excited electrons generates heat.

Among various carbon-based absorbers investigated to date, graphite[24], hollow carbon spheres[50], and reduced graphene oxides[52] (Figure 1-1) are promising candidates because of their high absorptance, low cost, and good processability. For example, a double-layered evaporation structure consisting of floating carbon foam and an exfoliated graphite solar-thermal converting layer on top has achieved 97% absorption

of solar radiation ranging from 250 to 2,250 nm[24]. The challenge to the future widespread application of carbon-based solar-driven interfacial evaporation is to reduce the associated cost.

Promising solutions include developing integrated evaporation system designs:

- Flame-treated wood[56].
- Low-cost absorbers such as polymeric sponges[57,58].
- Advanced manufacturing techniques such as three-dimensional printing[43].

Compared with single-component carbon absorbers, carbon-based composites that are magnetically responsive and optically active would enable easy recycling of the solar-thermal converting materials[50] and offer added functionalities such as photocatalytic treatment of organic pollutants[59].

1.2.1.2 Nanoscale plasmonic absorbers

They have demonstrated efficient and localized thermal energy conversion capability[25,60], and have been used for solar-driven evaporation as well[61,62,63,64]. Under resonant illumination by laser light, the plasmon-excited electrons are non-radiatively damped through the Landau damping instrument and redistribute their vitality through electron-electron and electron–phonon scattering forms to produce heat with a light-to-heat change productivity near to 100%[25,60].

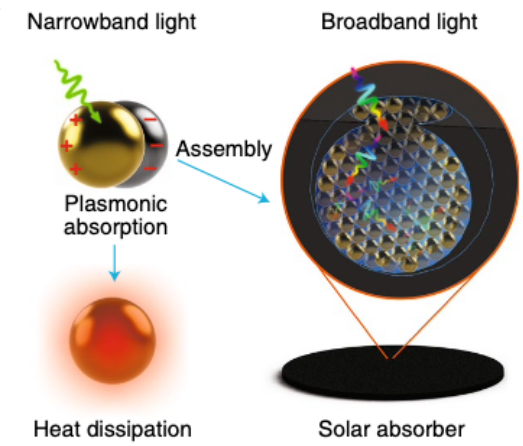

Figure 1-2 Schematic working principles of photothermal conversion for plasmonic-based solar absorbers. An individual plasmonic NP absorbs light at a distinct wavelength with narrow bandwidth, and electrons are excited and then relaxed to dissipate energy as heat. Self-assembled structures of plasmonic NPs can absorb broadband light due to the plasmonic coupling between the NPs.

Unlike carbon materials, individual plasmonic nanoparticles (NPs) such as Au only absorb a narrow band of light around their resonance peak. To cover a more comprehensive portion of the solar spectrum, NPs with distributed sizes can be assembled into porous films (Figure 1-2). Moreover, self-assembled NP films deposited on paper[54,65] and other substrates[27,53] have been used for solar-driven interfacial evaporation. The rough cellulose fibers of the supporting paper substrate help enhance the light absorption by the Au NPs from 65% for flat self-assembled films to 85% for paper-supported films within the 400–800 nm wavelength extend along a multi-scattering impact[65]. Ultrahigh absorption (~99%) was achieved by depositing metallic NPs on the surface of the nanoporous anodized aluminum oxide (AAO) template through a physical vapor deposition process[53]. The localized surface plasmon resonance coupling between neighboring particles with different shapes and sizes dramatically increases the density of optical modes and broadens the absorption wavelength. In addition, the porous AAO template plays a vital role in enhancing light absorption through an internal trapping effect and in reducing reflectance losses by reducing the refractive index mismatch with air. As a new category of photothermal converting material, new plasmonic absorbers, such as transition metal nitrides[66,67], with broad light absorption bandwidth, low cost, and, most importantly, high-temperature durability, have been explored to fulfill the need of solar-thermal applications.

1.2.1.3 Ideal solar absorbers

Ideal solar absorbers should have contrasting properties of high solar absorptance (0.25–2.5 μm) and low thermal emittance, which can be achieved through high reflectivity in the long-wavelength infrared region (2.5–25 μm). Solar absorbers can lose heat via thermal radiation, and such radiative losses can be significant, especially at higher temperatures. Decreasing the thermal emittance of the absorbers suppresses these radiative losses. A particular set of materials with these properties are spectrally selective solar absorbers, which at the same time have high solar absorptance and low thermal emittance.

1.2.2 Evaporation structure

Localizing solar-thermal heat generation to the air/liquid interface is essential to achieving high evaporation performance and high solar-to-vapor energy conversion

efficiency. One straightforward strategy to achieve interfacial heating is to float the solar absorber at the air/liquid interface either via its surface hydrophobicity, low density, or the usage of buoyant, porous materials such as carbon foams[24], air-laid papers[54,65], reduced graphene oxide aerogel[52] or AAO substrates substrates[27,39,53].

Efficient water supply to the solar heating region is critical to high-efficiency interfacial evaporation. For porous floating evaporation systems, the capillary wicking effect of the porous evaporation structure has been used to pump water. Porous microstructures with small pore sizes amplify the capillary pumping of water towards the heating region. Micrometer-sized pores have been shown to be more appropriate than nanopores for efficient capillary pumping of water[51]. In these floating evaporation systems, closed pores also help reduce the thermal conductivity of the interfacial structure, thereby restricting the generated heat from thermally diffusing to the bulk water and surrounding environment[24]. For the interfacial evaporation systems that are supported by the floater, such as polystyrene foam with closed pores, external fabric wicking materials are used to deliver water[49]. Besides appropriate pore sizes, achieving a strong pumping effect also requires the wicking materials to have good wettability with water.

The floating evaporation structure can move together with the receding air/water interface for continuous operation. However, it should be clarified that floating is not a necessary condition for realizing interfacial evaporation even though most of the reported evaporation systems have a floating evaporation structure. Localized heating at the air/water interface was also achieved recently when polystyrene spheres with a high scattering cross-section were intentionally mixed with Au NPs to trap the incident light within the top fluid layer through the strong multi-scattering effect. This scattering effect localized heat generation closer to the evaporation surface, increasing the evaporation temperature and rate[69]. The separated NPs for scattering and absorption provided additional flexibility in tuning solution-based systems and reduced the usage of expensive noble metals. Surface wettability of the evaporation structures plays an essential role in enabling interfacial evaporation and also influences evaporation performance:

- On the one hand, hydrophobic surfaces help float solar absorbers. Some examples include self-assembled Au NP films[70], hollow carbon spheres[50], and graphene sheets[51] at the air/water interface.
- On the other hand, hydrophilic surfaces are desired to wick water for evaporation, and stronger hydrophilicity leads to better capillary pumping capability[24].

Free-standing interfacial evaporation structures can have separate wettability properties on the top and bottom surfaces. By changing the ligands on the surface of AAO-supported assembled Au NP films, the impact of top and bottom surface wettability on evaporation performance has been investigated[72]. The wettability of the top surface has a negligible influence on the evaporation kinetics and evaporation rates, but that of the bottom surface strongly affects the evaporation performance. The hydrophilic bottom surface can be fully wetted by the underlying water to continuously and stably vaporize the liquid at high rates. In contrast, with a hydrophobic AAO bottom layer, the top solar-thermal converting layer cannot be wetted, thus limiting heat conduction to the liquid. Meanwhile, many bubbles formed around the bottom layer of AAO during the evaporation process. These thermally insulating bubbles severely restricted the heat and mass transfer, firmly lowering the evaporation rate. Under intense solar illumination, the formed bubbles further grew and eventually ruptured the solar-thermal converting films.

1.2.3 Thermal insulator design

Appropriate thermal insulation design is critical to localize heat at the air/water evaporative interface, reduce heat losses and improve evaporation efficiency. The downward conduction loss is dependent on the thermal conductivity of the insulator (k) and can be estimated by,

$$q_{water} = -kAdT / dx \qquad \text{(Eq 1-1)}$$

Where A is the surface area of the solar absorber facing the sun, dT/dx is the temperature gradient from the solar absorber to the underlying water.

Therefore, the upward convection and radiation loss might be hypothetically assessed with the measured temperature of the evaporation surface. To decrease descending conduction heat loss from the solar absorber to the fundamental water body that happens within the single-layered evaporation system, a thermally insulating layer made of porous carbon foam can be introduced, such as in the double-layered evaporation structures[24] (Figure 1-3).

- The closed pores in the porous carbon foam contained air, which significantly reduced the heat conduction.
- The foam, however, also included open pores needed to deliver fluid to be evaporated, and the wetted foam has a higher thermal conductivity than the dry one.

In a recent study[29], a solar absorber was placed on a thermal insulator (polystyrene foam) that only has closed pores. The foam was wrapped with hydrophilic cellulose, and water was pumped towards the heating surface through the capillary wicking effect in the cellulose. In another recent study, the downward thermal leakage was almost eliminated by using close-pored thermal insulation with a few drilled holes to allow for liquid delivery[49]. In this case, the contact range between the evaporation surface and the water body is minimized, and the overwhelming heat misfortunes move to the top surface.

An ideal evaporation structure should have not only low thermal emittance but also high thermal reflectance at the wavelength where water emits; that is, the reflectivity in the infrared spectrum should be elevated to block water from emitting thermal radiation. This requirement creates additional challenges in evaporating water, which must be exposed to the ambient air for evaporation to occur.

1.2.4 Solar-to-vapour conversion efficiency measurements

Evaporation efficiency is a key performance metric that is linearly dependent on evaporation rate (ṁ) and is characterized as the proportion of stored thermal vitality within the produced vapor to the incoming solar flux (which is, solar-to-vapour conversion efficiency, η_{sv}),

$$\eta_{sv} = \dot{m}hLV / q_{solar} \quad \text{(Eq 1-2)}$$

Where hLV is the total evaporation enthalpy change that includes sensible heat and phase-change enthalpy, q_{solar} is the incident solar flux. Single-layered dissipation structures generally have low dissipation proficiency (from around 40 to 50%) due to unsuppressed heat losses to the bottom water and surrounding air. In contrast, double-layered structures have much higher conversion efficiency, and the highest solar-driven interfacial evaporation efficiency is ~90%. The wide extent of proficiency among distinctive interfacial dissipation systems is primarily established within solar absorption and thermal insulation plan distinction.

To achieve high evaporation efficiency, the evaporation system should efficiently absorb the broadband solar light and adopt a thermal insulation design to minimize various forms of heat loss. Theoretically achievable efficiency for specific systems can be estimated by deducing heat losses from the evaporation systems at their operating temperatures. Evaporation efficiency dependence on solar flux varies with detailed thermal insulation design. In evaporation systems with good thermal insulation, evaporation efficiency increases with solar flux as the ratio of the heat losses to the solar flux decreases. When changing from one sun (1 kW m^{-2}) to concentrated solar radiation (2 kW m^{-2}), the small drop of evaporation efficiency could possibly be related to optical losses during solar concentration[24,27].

Most of the efficiencies reported are the steady-state evaporation efficiency, which is calculated using the steady-state evaporation rate. It takes, however, different times for different systems to reach their steady states. To consider the time dependence, some scientific papers recommend that the time-averaged evaporation efficiency with the exact duration of solar illumination should be reported as well. It will incorporate the reaction time for the framework to reach the consistent dissipation rate. The quick reaction would advantage the aggregate dissipation execution beneath irregular solar radiation conditions such as on cloudy days. In addition, the evaporation experiment should ideally be conducted on an open body of water without requiring extra sophisticated thermal insulation from a container, which is one of the key advantages of solar-driven interfacial evaporation. High-accuracy estimation of physical parameters (Figure 1-3), counting the temperature of solar absorber surface, vapor temperature and control thickness of sun-powered light, is another prerequisite for precise assessment of the evaporation execution.

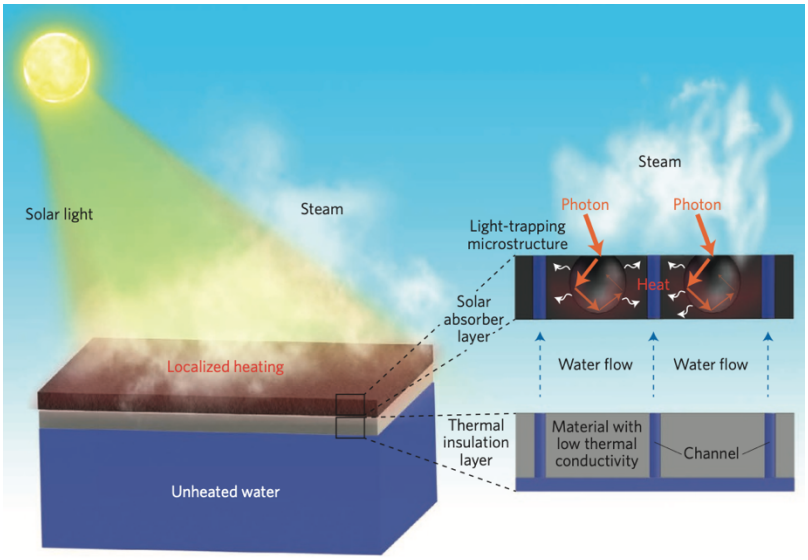

Figure 1-3 Schematic of the structure and operation of an interfacial steam generation system floating at the water-air interface. Solar light is absorbed by the absorber layer and converted into thermal energy, which heats up the water at the interface. The thermal insulation layer consists of material with low thermal conductivity and helps confine the heat at the interface. The channels within the thermal insulation layer and the solar absorber layer transport the unheated water to the heated interface for the generation of steam. The insets show the conversion of photon energy to heat in the absorber layer and the transportation of water in both the absorber and the thermal insulation layer.

Chapter 2 Components & Specifications

2.1 Transparent cover – Transparent bubble wrap

The transparent cover is placed on the top surface of the solar-driven interfacial dissipation framework to avoid losses of heat basically by means of convection and radiation (Figure 2-1). The transparent bubble wrap cover transmits sunlight and reduces by >50% the convective heat losses. Even the cover is optically transparent, one possible limitation from such a strategy is the unavoidable optical loss of incident solar light.

Figure 2-1 Transparent cover

2.2 Spectrally selective solar absorber

The solar absorber can efficiently absorb and convert the solar radiation into heat with minimized radiation loss (Figure 2-2). The low thermal emittance is obtained by using an infrared-reflective metal as the substrate that is exceptionally reflective at middle and far-infrared wavelengths. The spectrally selective solar absorber consists of a cermet-type absorber coated on a copper shit; metal NPs are immersed with the ceramic binders to absorb solar radiation while at the same time having high transmission in the infrared region. Multilayered composite absorbers are used to decrease the reflectance from the absorbing layer to reach high absorptance (>0.9). Moreover, an antireflection coating (ARC) also decreases the reflection of solar light.

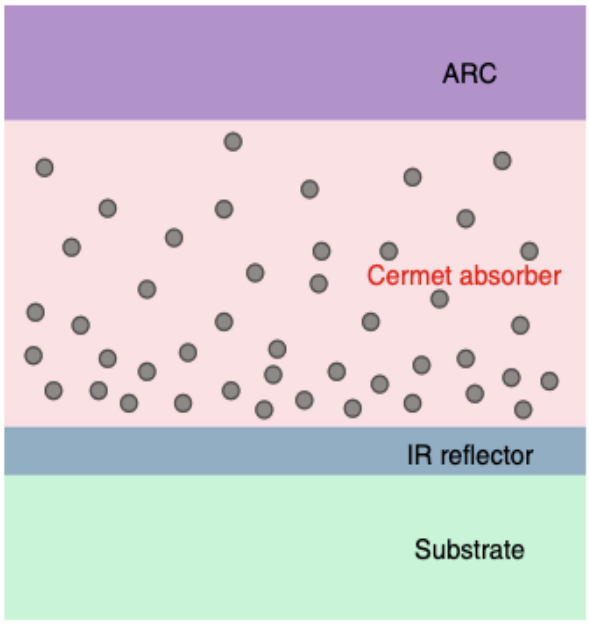

Figure 2-2 Schematic structure of the spectrally selective solar absorber. Composition: antireflection coating (ARC), selective absorption layer, and infrared (IR) reflection layer and a supporting substrate.

The spectrally selective solar absorber has a high solar absorptance of 0.93 and a low emittance of 0.07 at 100 ˚C, which suppresses the radiative losses. The surface radiation loss has been lowered by more than 90% by replacing blackbody absorbers with low-emittance, spectrally selective solar absorbers. It is important to mention that commercial spectrally selective absorbers are usually solid coating; consequently, the management of water supply and vapor transport needs a different approach.

2.3 Evaporation structure – Copper porous foam & Preparation

The evaporation structure is key in the 3D porous solar-driven evaporation design since the solar-thermal heat generation is localized to the air/liquid interface to achieve high evaporation performance and high solar-to-vapor energy conversion efficiency (Figure 2-3). Basically, this material was utilized to build the porous evaporation chamber due to its elevated thermal conductivity and wide accessibility. Table 2-1 shows the parameters and values used for the copper porous foam in COMSOL Multiphysics software. To reach high-efficiency interfacial evaporation, water must be supplied efficiently to the solar heating region. One way to pump water is by the capillary wicking effect of the porous evaporation configuration. The other way is by

the wicking material, which will be explained as the next component. Porous microstructures with compact pore size magnify the capillary pumping of water towards the heating region. In this design, micrometer-sized pores are chosen since they report an efficient capillary pumping of water. In addition, the closed pores reduce the thermal conductivity of the evaporation mentioned above structure.

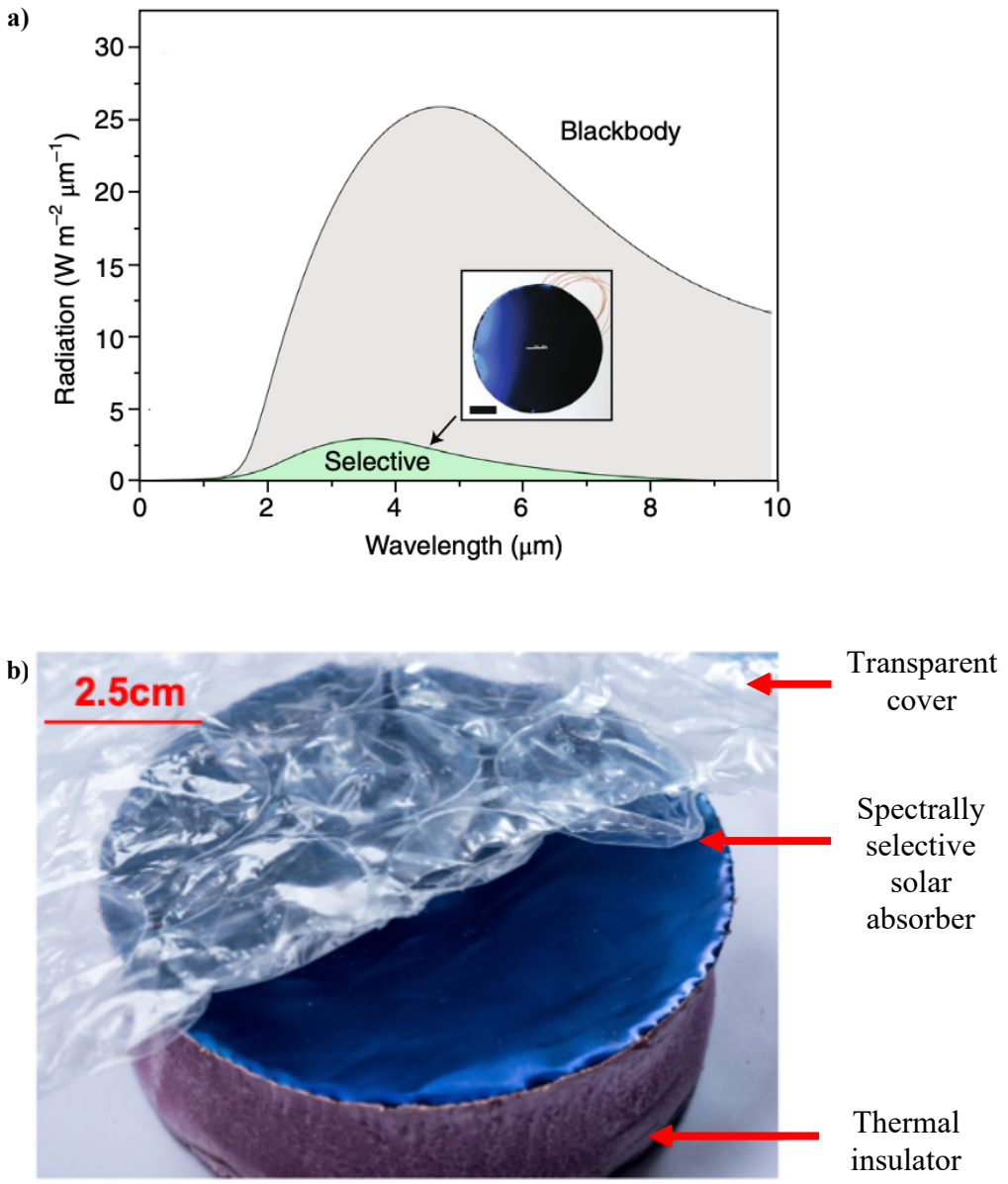

Figure 2-3 **a)** Comparison of radiation heat loss from a blackbody absorber and the spectrally selective absorber at 100 ˚C. **b)** A photograph of bubble wrap, spectrally selective coating and thermal insulator.

The copper porous foam is set to different wettability properties on the top surface is hydrophobic, and the bottom surface is hydrophilic (Figure 2-4). The reason is that

the wettability of the top surface has a minimal influence on the evaporation kinetics and evaporation rates. Nevertheless, the bottom surface strongly improves the evaporation performance. Moreover, the surface wettability of the evaporation structures plays a critical part in permitting interfacial evaporation additional impacts dissipation capabilities as the hydrophobic surface allows to float the solar absorber and the hydrophilic, allow to wick water for evaporation.

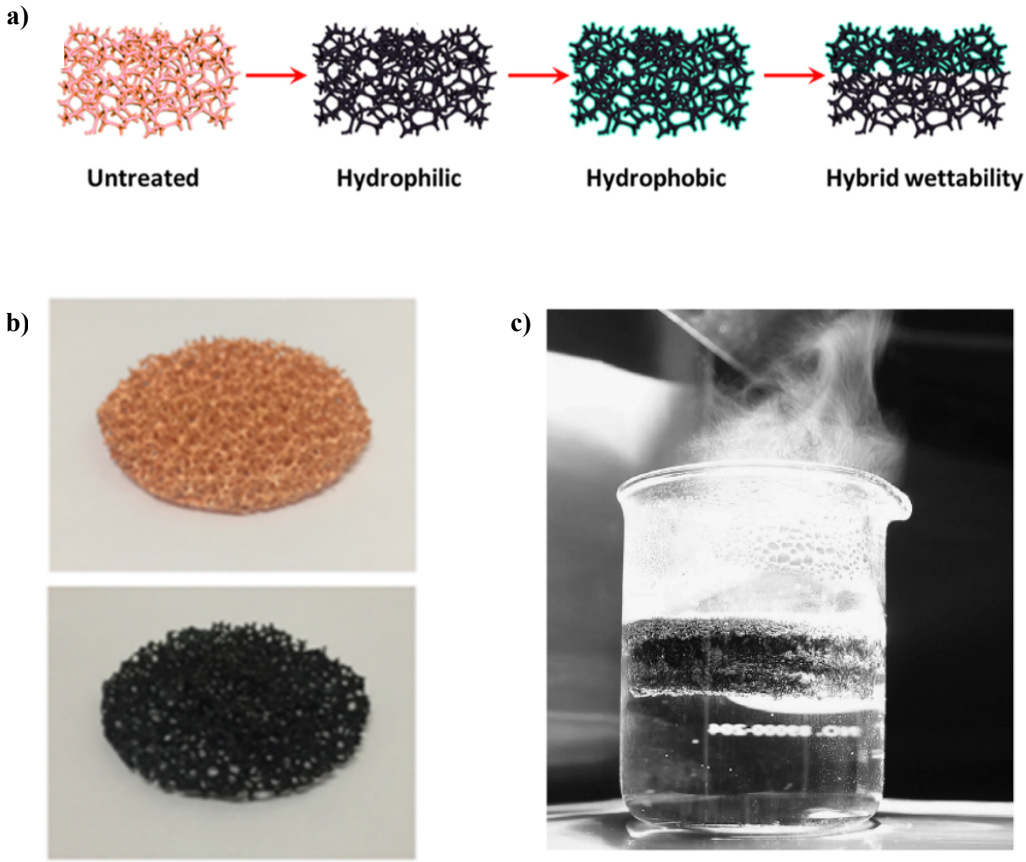

Figure 2-4 **a)** Schematic process with different surfaces wettability for preparing copper foam. **b)** A photograph of untreated copper foam (top) and treated hydrophilic copper foam (bottom). **c)** A photograph of enhanced steam generation by the treated hydrophilic copper foam under the solar illumination of 10 kW/m^2.

The hydrophilic surface is submerged by the underlying water to constantly and stably vaporize the liquid at high rates. The hybrid copper foam is prepared by a three-step surface treatment of pristine commercial foam. Initially, the foam is cleaned by acetone, ethanol, and deionized water through sonication before the preparation.

- Firstly, the surface of the copper foam is submerged and oxidized by a mixed strong alkali solution (0.065 M K2S2O2 and 2.5 M KOH at 60 ˚C) during an hour to become hydrophilic.
- Secondly, the obtained foam is deposited with a fluorinated silane through a vapor deposition process to convert the surface into hydrophobic. 1H,1H,2H,2H-perfluorooctyltri-cholorosilane is loaded into a plastic vacuum chamber to obtain the mentioned surface.
- Thirdly, half of the hydrophobic copper is submerged again in the first solution to convert that portion into hydrophilic.

Table 2-1 Copper porous foam information

Parameters	**Values**
Porosity	0.92
Pore radius	6.8E-7 m
Permeability	5.3E-14 m^2
Density	1318.4 kg/m^3
Heat transfer coefficient	30 $W/(m^2K)$
Volume fraction	0.04
Diffusion coefficient	2.8E-10 m^2/s
Initial moisture concentration	63376 mol/m^3
Mass transfer coefficient	2.5 mol/m^3
Water concentration	55600 mol/m^3

2.4 Wicking material – Air-laid paper

The following component function is used to deliver water to the evaporation region. Other than suitable pore sizes, accomplishing a strong pumping effect at the same time requires the wicking materials to have outstanding wettability with water. Therefore, air-laid paper supplies water efficiently to the solar heating region in order to achieve high-efficient interfacial evaporation. It is proven that this material can provide sufficient water supply to compensate for the evaporation mass loss. The

theoretical maximum evaporation mass flux is 1.584 kg/(m^2h) under 1-sun illumination, and the water sorption rate of the wicking material is 35.84 kg/m^2h, favorable. In fact, the wicking material will become more hydrophilic after absorbing water; consequently, the resultant water sorption will be even higher. Figure 2-5 a) shows that the air-laid paper is completely wetted by the red aqueous solution that contains Rhodamine dye within 30 seconds.

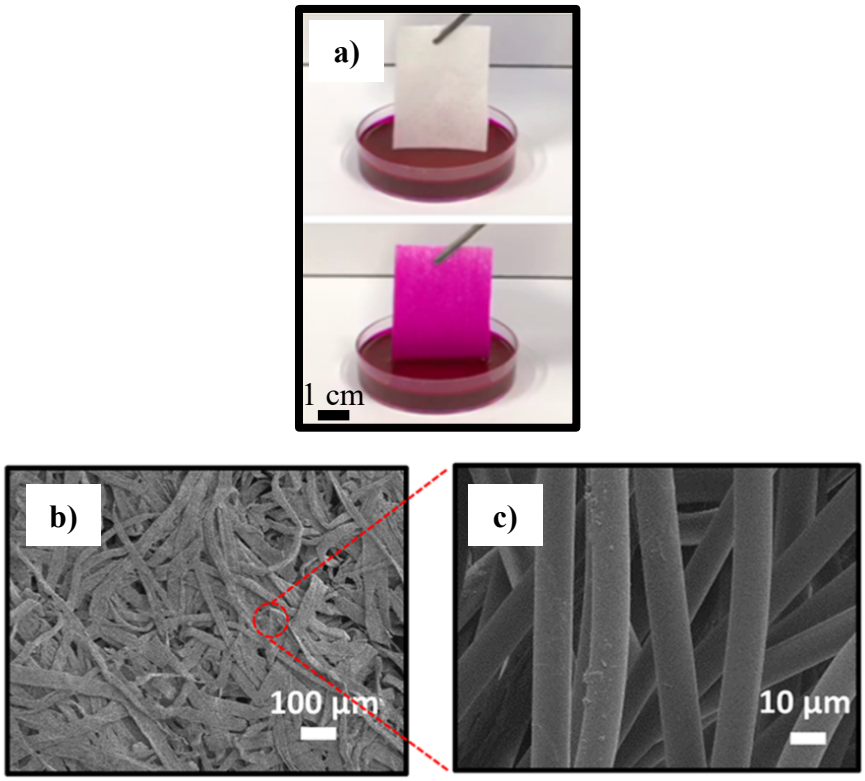

Figure 2-5 **a)** Water-wicking test of air-laid paper. **b)** SEM image of the air-laid paper under 100 µm showing its porous structure. **c)** SEM image of the air-laid paper under 10 µm showing its fiber component.

2.5 Thermal insulation – Polystyrene & EPE foam

The thermal insulation floating foam is made of polystyrene with only closed pores because the air-laid paper delivers the water. The foam mentioned above has two main purposes: first, to reduce downward conduction heat loss from the solar absorber to the underlying water body since its thermal conductivity is 0.03 W/mK; second, as both the physical separator and floater of the structure. In addition, expanded

polyethylene (EPE) foam is composed of small-closed cells that evenly hold ties together which makes the foam also have very low permeability (Figure 2-6). Consequently, EPE foam is used to wrap the entire evaporator in order to reduce heat leakage from the sidewalls.

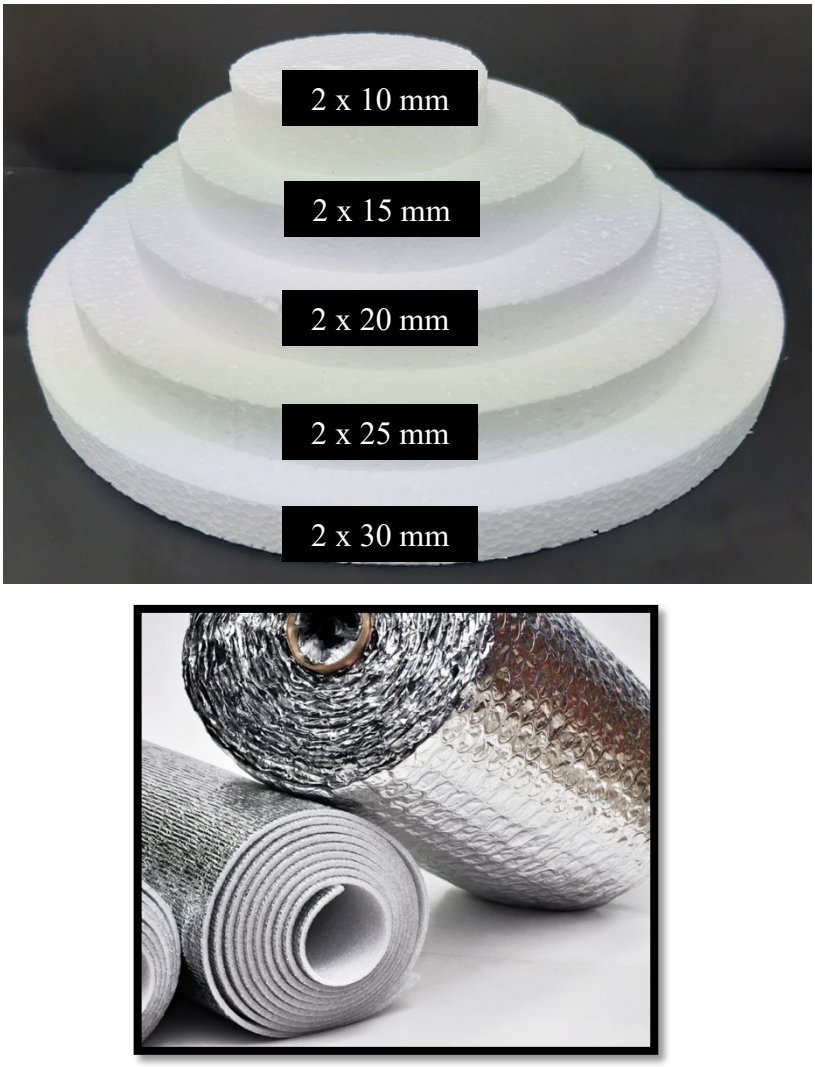

Figure 2-6 a) A photograph of polystyrene foam with different diameters. b) A photograph of expanded polyethylene (EPE).

Chapter 3 3D Copper Porous Solar-Driven Evaporation Design

The 3D porous solar-driven evaporation design contains six crucial components: Table 3-1 shows the shape and dimension of each component, and Figure 3-1 shows a 2D axisymmetric and 3D view of the design from COMSOL Multiphysics software. First, a transparent bubble wrap cover, cylinder shape, is employed to avoid losing heat by means of convection and radiation. Second, a spectrally selective solar absorber, half ellipse shape, is used to absorb and convert more efficiently the solar radiation into heat with minimized radiation loss. Third, the different wettability properties of copper porous foam, unique shape in order to fit the spectrally selective solar absorber's shape, provide suitable space for vapor generation. Fourth, an air-laid paper – which is placed between the copper porous foam and thermal insulation floating insulation, and in the middle of each layer of the thermal insulation floating insulation – is utilized basically to automatically pump water from the reservoir at the bottom to the solar-heating region. Fifth, six polystyrene foams, cylinder shapes, are located at the bottom to reduce downward conduction heat loss and to float the evaporator. Sixth, an EPE foam is employed to wrap the entire structure to reduce heat leakage from the sidewalls.

Table 3-1 Solar-driven evaporation design dimensions

Components	Shape	Dimensions (mm)
Transparent bubble wrap cover	Cylinder	5x80
Spectrally selective solar absorber	Half ellipse	10x40
Copper porous foam	Special	10x80
Air-laid paper	Cylinder	1x80
5 Air-laid paper	Shit	0.2x80
6 Polystyrene foam	Ring cylinder	30x13, 30x26, 30x39,30x52, 30x65 and 30x78

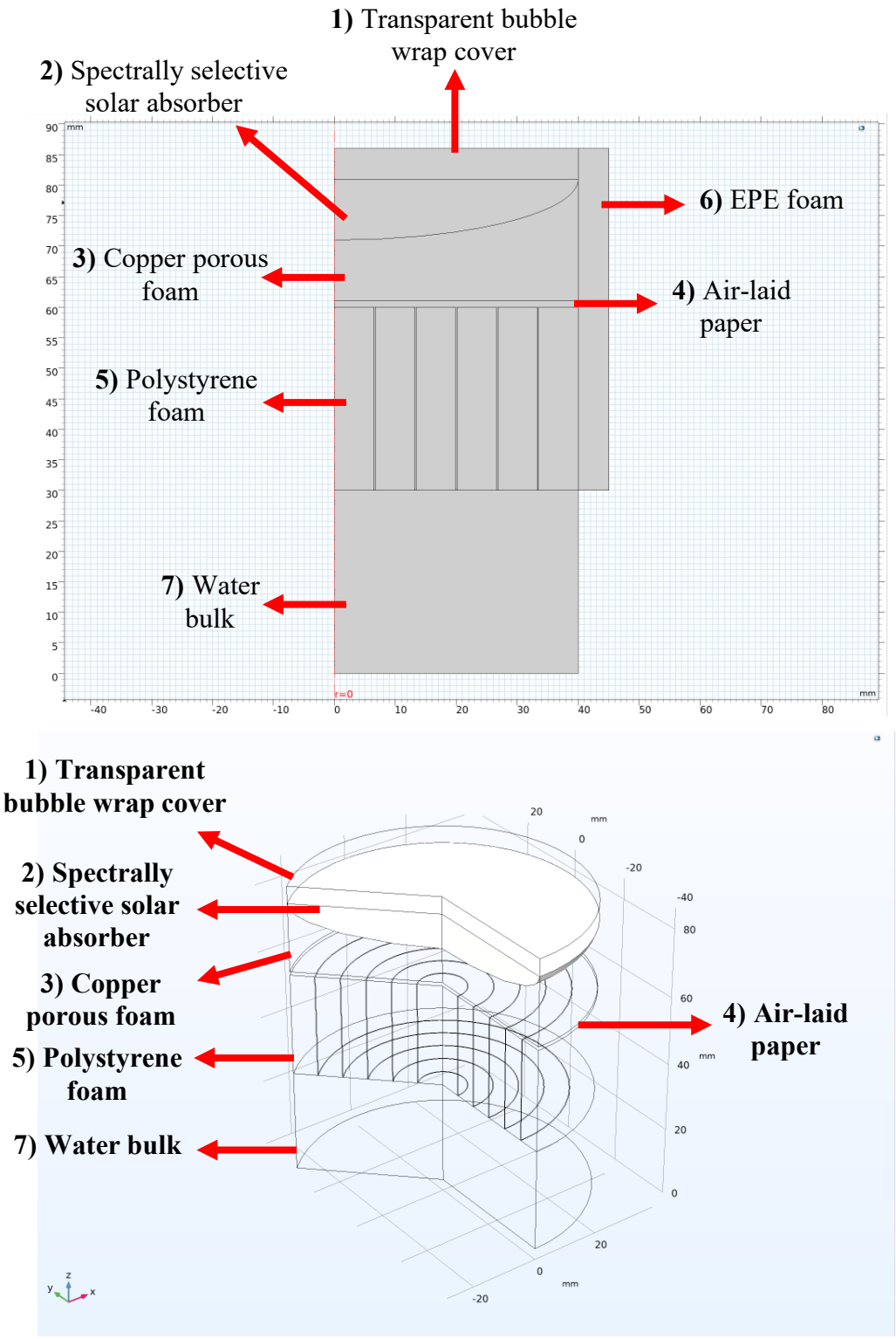

Figure 3 a) 2D axisymmetric view of the design. b) 3D view of the design.

Chapter 4 Results and discussion

The 3D porous solar-driven evaporation design minimizes heat losses; therefore, it is possible to produce high-efficiency steam under 1 sun solar flux (1 kW/m^2). When the ratio of the thermal concentration is greater than 200 with the solar-to-steam conversion efficiency near 20%, the evaporator generates steam.

In a straightforward design, as shown in Figure 4-1, convection and radiation from the upper layer create a loss in the converted solar-thermal energy. In addition, downward conduction creates a loss of converted heat. Moreover, the thermal concentration proposed depends on concentrating the harvested solar-thermal energy respecting a compact dissipation region to boost the vapor temperature. Therefore, the plan mentioned above limits the accessible surface region for water evaporation, and the suppressed evaporation, in turn, causes overheating of the spectrally selective solar absorber.

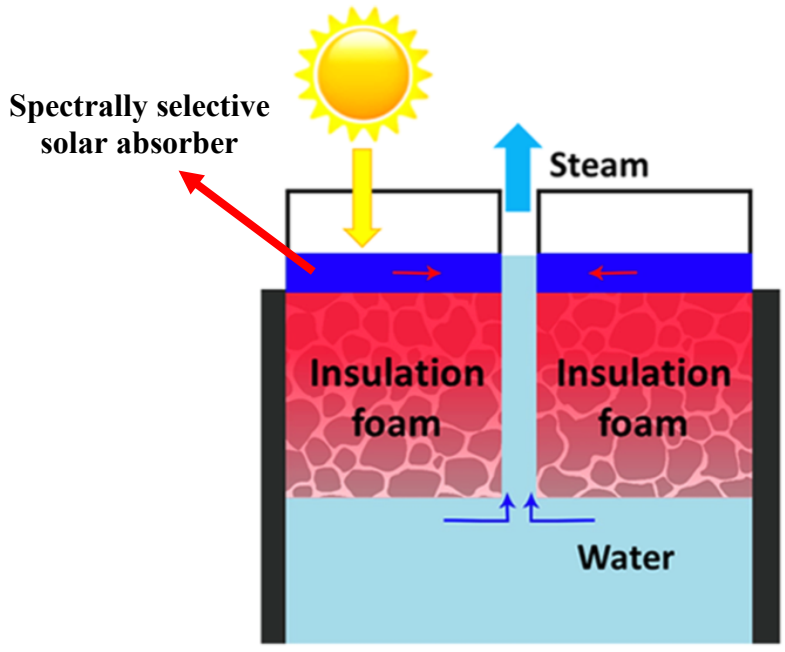

Figure 4-1 Schematic structure of a straightforward thermal concentrated interfacial evaporator with a small hole in the center which allows the escape of the generated steam.

The proposed 3D copper porous solar-driven evaporation design amplifies the evaporation area since the copper porous is placed between the spectrally selective solar absorber and the water-supplying layer. By adapting the surface wettability of the copper porous foam, the evaporation mass could be improved to guarantee steam generation at 100 ˚C. With expanded dissipation flux that keeps the changeover solar-thermal energy as inactive heat within the hot steam, the surface temperature of the spectrally selective solar absorber; consequently, the heat losses from the evaporation structure are reduced. An additional particularity of design is the steam outlet, that is compacted and placed at the sidewall (Figure 4-2, 4-3). The unique design benefits are to evade potential blocking of solar sun incidence onto the spectrally selective solar absorber by the created steam and promote the steam collection.

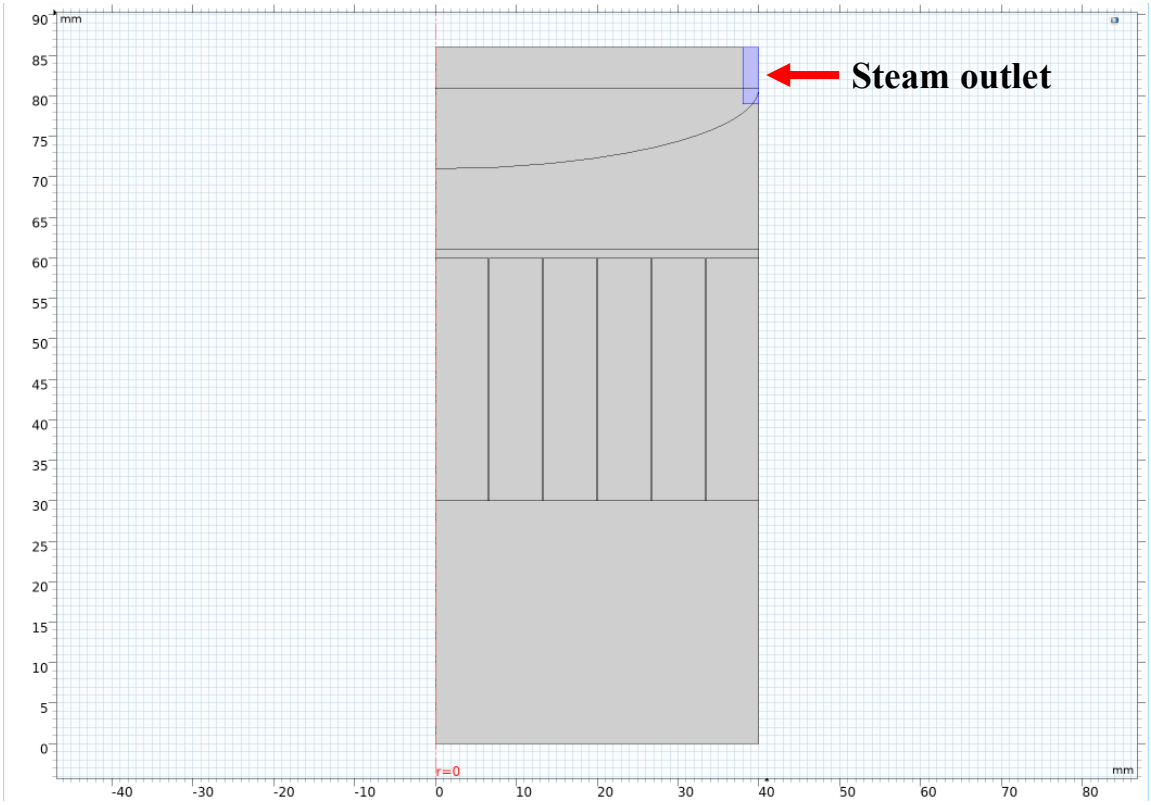

Figure 4-2　2D axisymmetric view of the design where the steam outlet is shown.

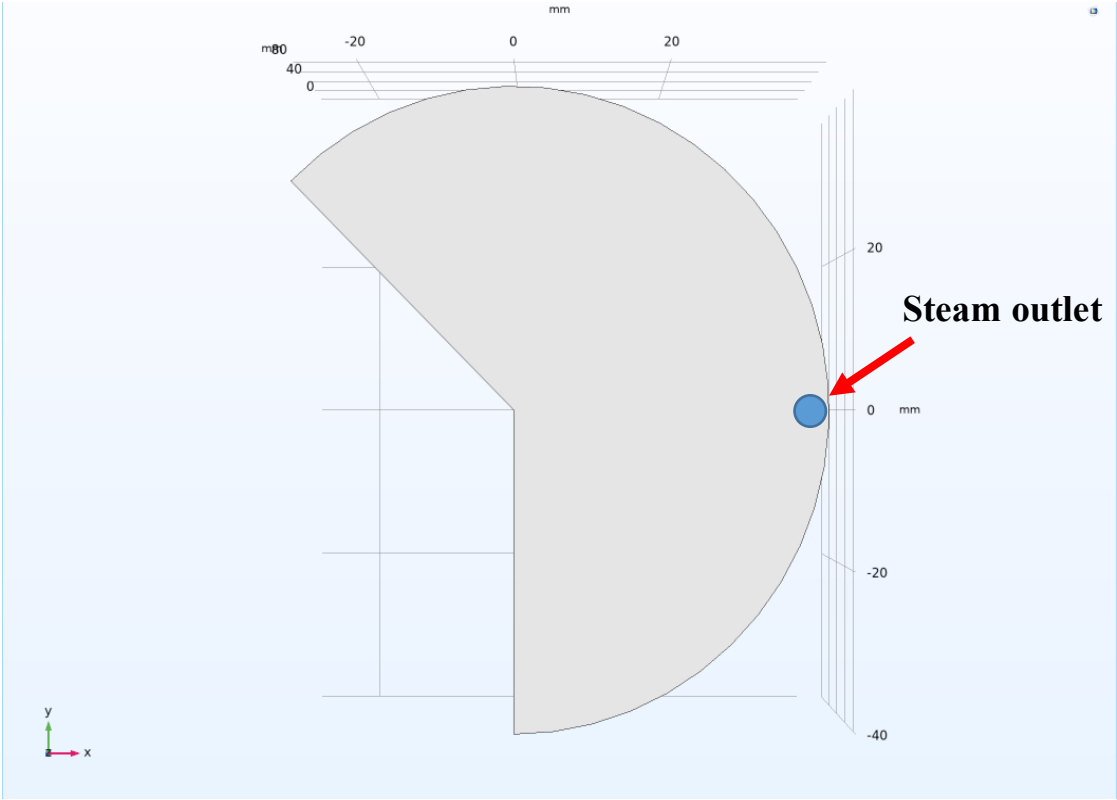

Figure 4-3 3D view of the design where the steam outlet is shown.

Each of the hydrophilic, hydrophobic and hybrid hydrophilic-hydrophobic copper was compared to analyze the evaporation performance of the evaporator structure. The preparation of the different surfaces was explained in Chapter 2. Figure 4-4 a) shows that the hydrophobic (black line) evaporator has appeared the quickest and highest vapor temperature rise, and come to a consistent temperature posterior to 1 sunlight for 1000 s – this indicates that the system has achieved a thermal balance with the atmosphere. In contrast, the hydrophilic evaporator (blue line) has the lowest vapor temperature and comes to a consistent temperature which does not reach the boiling point of water. The hybrid hydrophilic-hydrophobic (red line) evaporator has the closest temperature to the boiling point of water and starts consistent steam generation after 1200 s. The principal goal is to generate steam when the evaporator surface temperature

achieves the boiling point of water, and the evaporation process enters the steady state. Figure 4-4 b) shows the reverse trend to the vapor temperature since the hydrophilic copper foam has the largest mass loss and the hydrophobic copper foam, the smallest mass loss. Moreover, Figures 4-5, 4-6 show the concentration distribution of the evaporator system at 1800 s and 3600 s in COMSOL Multiphysics software.

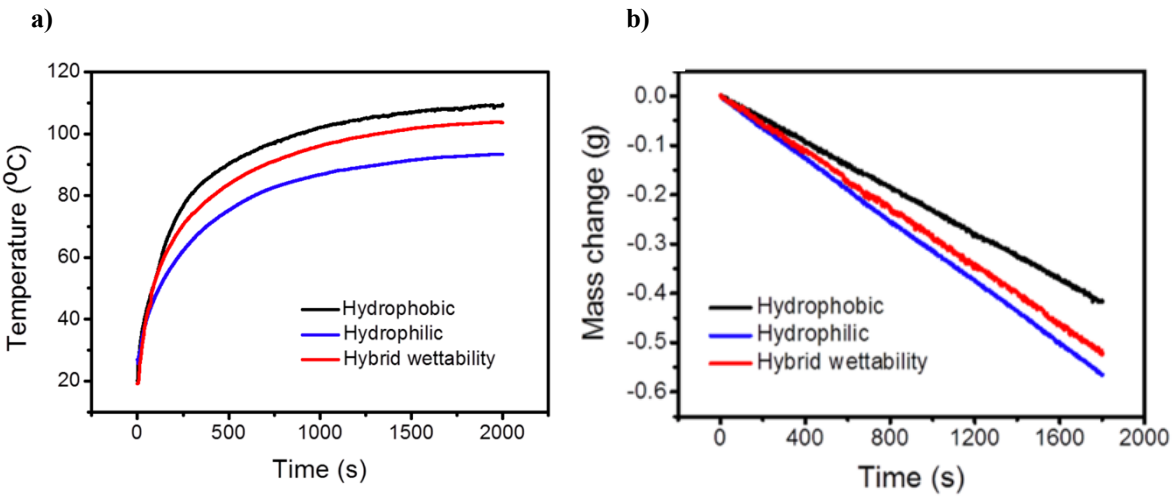

Figure 4-4 **a)** Temperature evolution of a spectrally selective absorber in steam generators with different surface wettability. **b)** Evaporation mass change for the three evaporators as a function of illumination time.

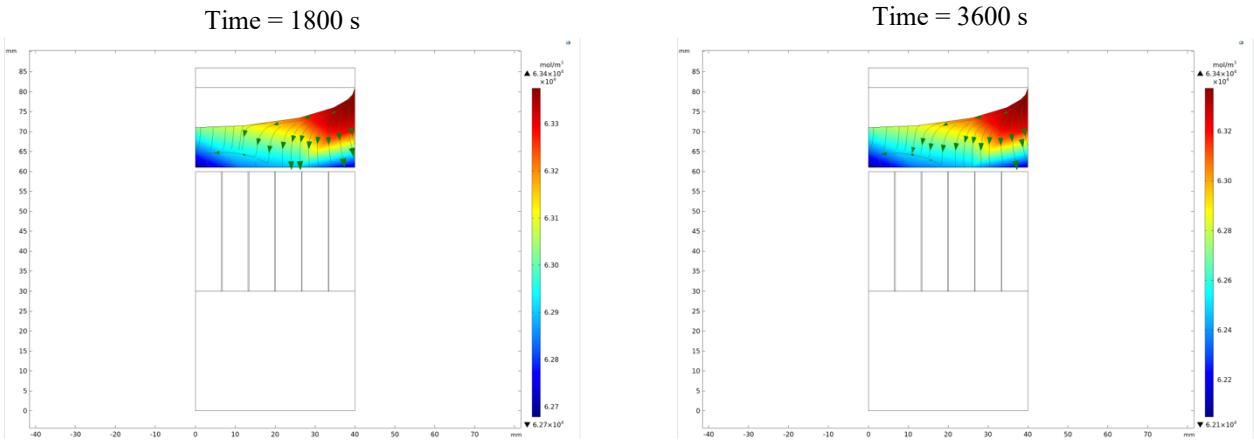

Figure 4-5 2D Axisymmetric concentration distribution of the evaporation system

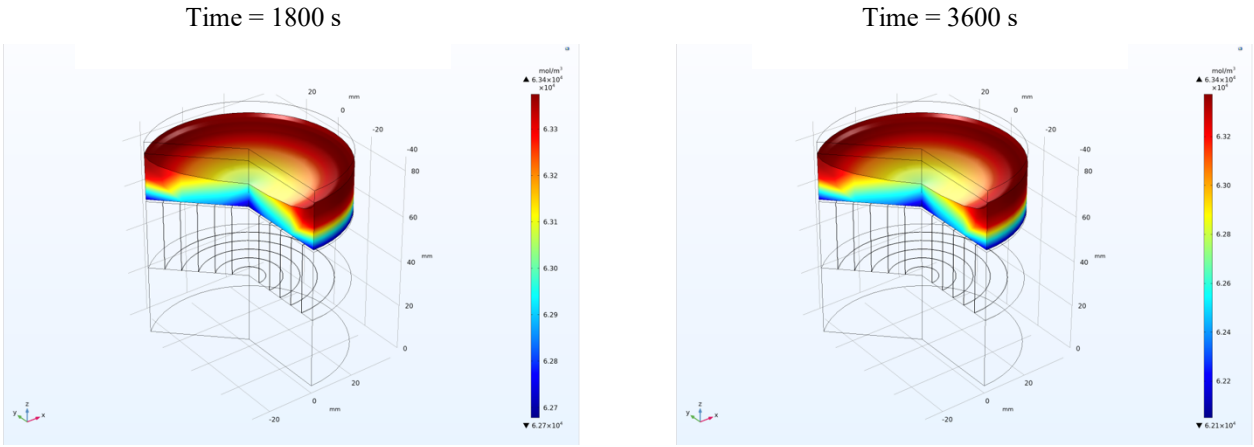

Figure 4-6 3D concentration distribution of the evaporation system

As previously mentioned, water supply is the main influence that determines the vapor temperature and evaporation efficiency. The hydrophobic copper foam, slow water supply, accelerates the increase of the vapor temperature to the steam; however, this restricts the evaporation efficiency. The hydrophilic surface, fast water supply, improves the evaporation flux, although it lowers the vapor temperature. Therefore, the hybrid hydrophilic-hydrophobic surface adjusts the evaporation performance. Based on the energy balance principle, it is possible to analyze the evaporation efficiency for the evaporation structure (Figure 4-7).

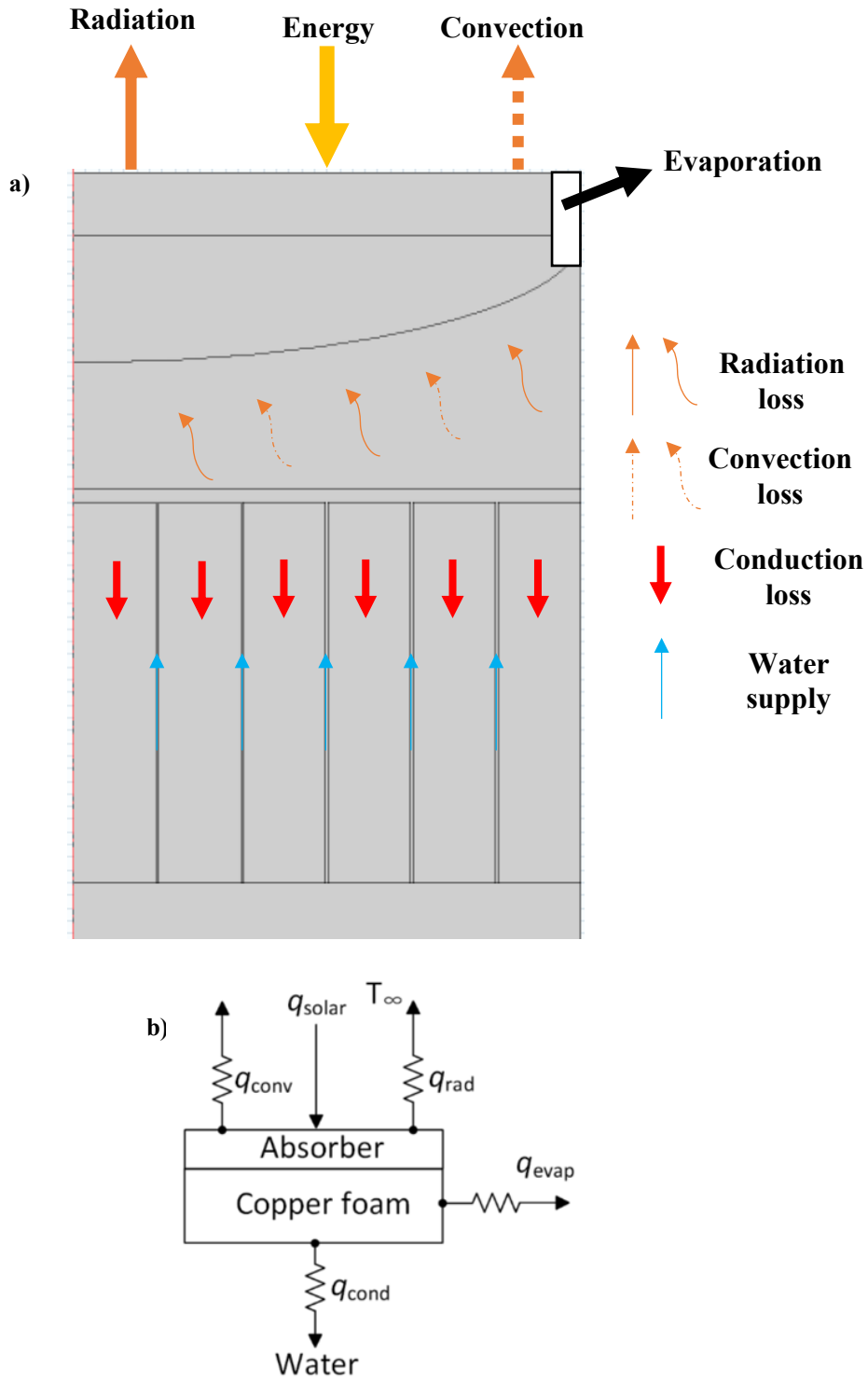

Figure 4-7 Theoretical heat loss analysis of 3D porous solar-driven interfacial evaporator. **a)** Schematic structure for the 3D porous interfacial evaporator. **b)** Schematic energy transfer diagram.

Consequently, the following equation can be obtained,

$$q_{solar} * T_{cover} * \alpha_{abs} = q_{rad\_abs} + q_{conv\_abs} + q_{cond\_water} + q_{evap} \quad \text{(Eq 4-1)}$$

Where T_{cover} is the transparent cover transmittance (0.90), α_{abs} is the spectrally selective solar absorber absorptance (0.93), q_{rad_abs} and q_{conv_abs} are the radiation and convection heat loss of the spectrally selective solar absorber, and q_{cond_water} is the conduction heat loss from the polystyrene foam to the water underneath. Moreover, it can be calculated by,

$$q_{rad\_abs} = \varepsilon_{abs} * \boldsymbol{\sigma} * (T_s^{\,4} - T_\infty^{\,4}) \quad \text{(Eq 4-2)}$$

$$q_{conv\_abs} = h_{abs} * (T_s - T_{cover}) \quad \text{(Eq 4-3)}$$

$$q_{cond\_water} = k_f * (T_{top} - T_{down}) / d_f \quad \text{(Eq 4-4)}$$

Where ε_{abs} is the emittance of the spectrally selective solar absorber (0.07), $\boldsymbol{\sigma}$ is the Stefan-Boltzmann constant 5.67*10E-8 W/(m^2K^4), T_s is the spectrally selective solar absorber temperature (100 ˚C), T_∞ is the ambient temperature (20 ˚C), T_{cover} is the temperature of the transparent cover (48 ˚C), h_{abs} is the convection heat transfer coefficient between the transparent cover and the spectrally selective solar absorber (5.8 W/m^2K), k_f is the thermal conductivity of the polystyrene foam (0.03 W/mK), and d_f is the thickness of the polystyrene foam (30 cm), T_{top} and T_{down} are the temperatures at the top surface and bottom surface of the foam mentioned above (77 ˚C and 21 ˚C) under 1 sun flux. The steam generation efficiency (η) is obtained by,

$$\eta = T_{cover} * \alpha_{abs} - (q_{rad\_abs} + q_{conv\_abs} + q_{cond\_water} + q_{evap}) / q_{solar} \quad \text{(Eq 4-5)}$$

Table 4-1 Heat loss analysis of 3D porous interfacial evaporator

Variable	Values
q_{rad_abs}	48.6 W/m^2
q_{conv_abs}	301.6 W/m^2
q_{cond_water}	5.6 W/m^2
η	**48.1 %**

Based on (Eq 4-5), the theoretical solar-to-steam conversion efficiency of the 3D porous solar-driven evaporation design is 48.1%, as shown in Table 4-1.

A 3D COMSOL Multiphysics simulation was generated for the structure in order to gain inside into the temperature evolution. Figure 4-8 shows the temperature evolution of the transparent bubble wrap cover, spectrally selective solar absorber, and polystyrene foam at 3600 s. Therefore, Figures 4-9, 4-10, 4-11, 4-12 show the 2D axisymmetric and 3D temperature distribution of the whole evaporation system for 1800 and 3600 seconds. It clearly appears localized heating at the spectrally selective solar absorber and the copper foam. After 1 sun illumination for 2 hours, the temperature of the copper foam reached 100˚C, demonstrating that the evaporator can effectively create steam.

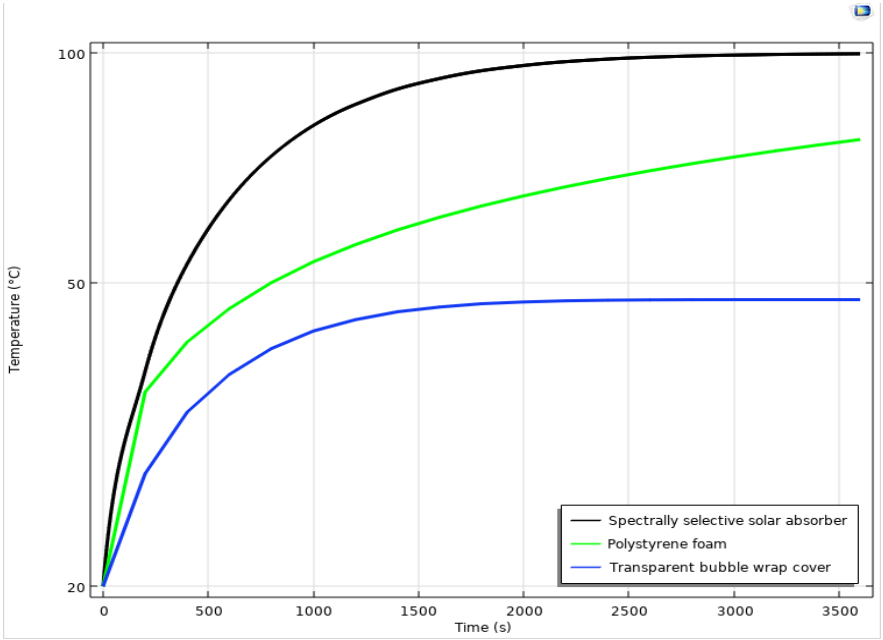

Figure 4-8 Temperature evolution of different components in the steam generator.

Figure 4-9 2D Axisymmetric temperature distribution of the evaporation system Time = 1800 s

a) Transparent cover b) Spectrally selective solar absorber c) Copper porous foam
d) Air-laid paper e) Water bulk

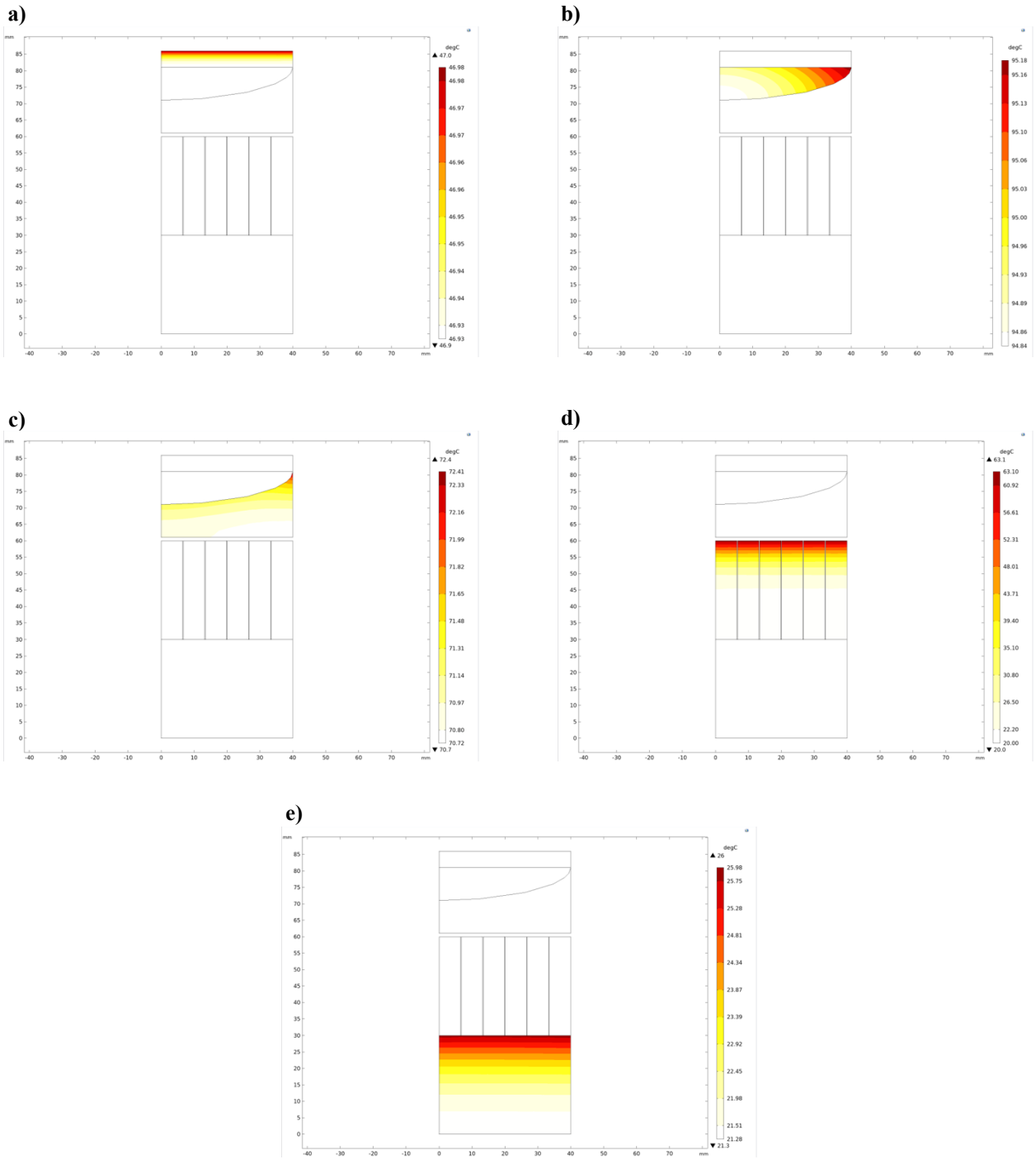

Figure 4-10 3D Temperature distribution of the evaporation system
Time = 1800 s

a) Transparent cover b) Spectrally selective solar absorber c) Copper porous foam
d) Air-laid paper e) Water bulk

a)

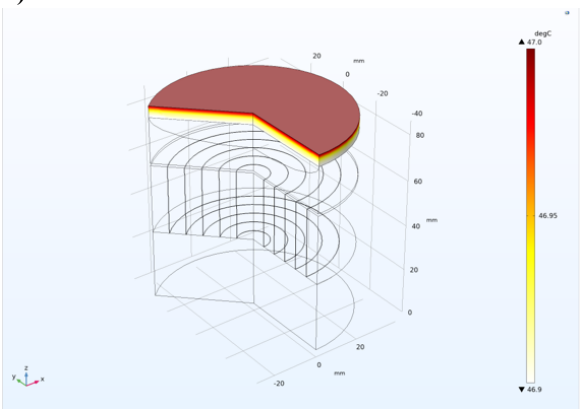

b)

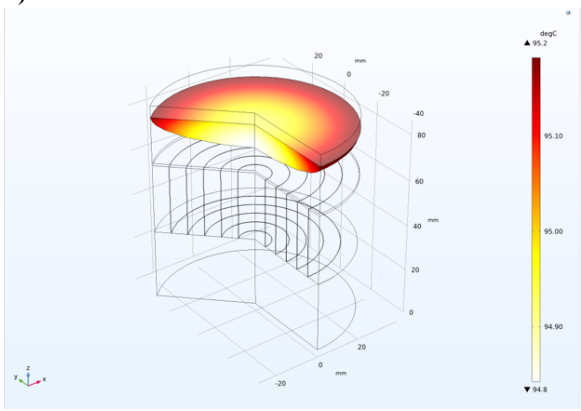

c)

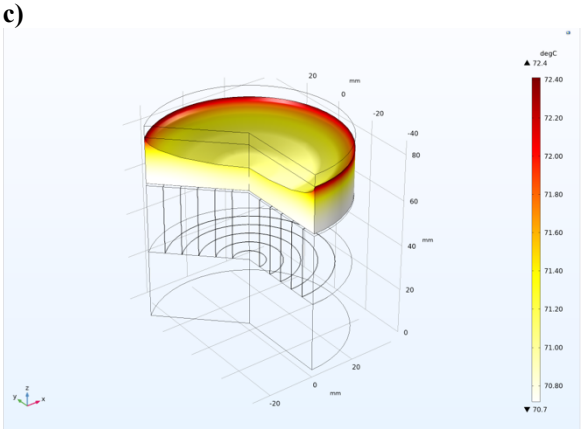

d)

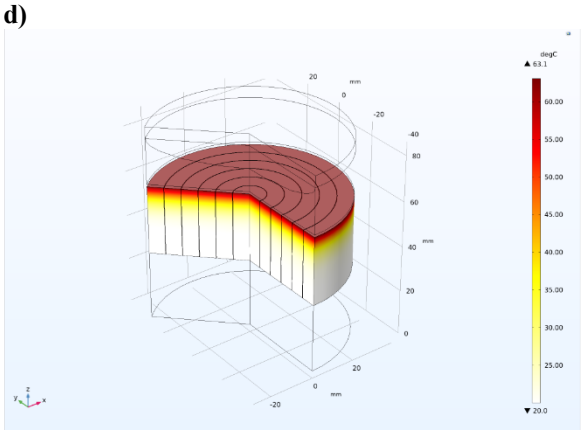

e)

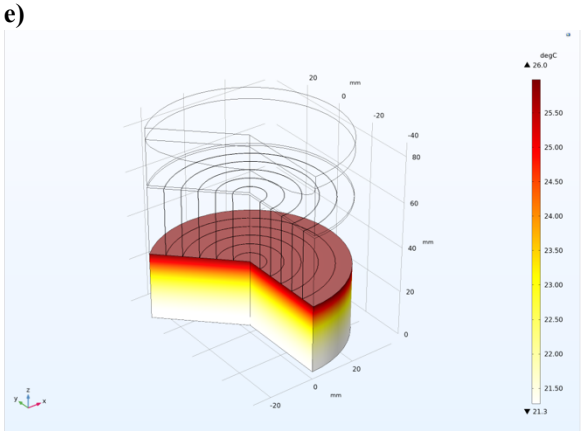

Figure 4-11 2D Axisymmetric temperature distribution of the evaporation system Time = 3600 s

a) Transparent cover b) Spectrally selective solar absorber c) Copper porous foam
d) Air-laid paper e) Water bulk

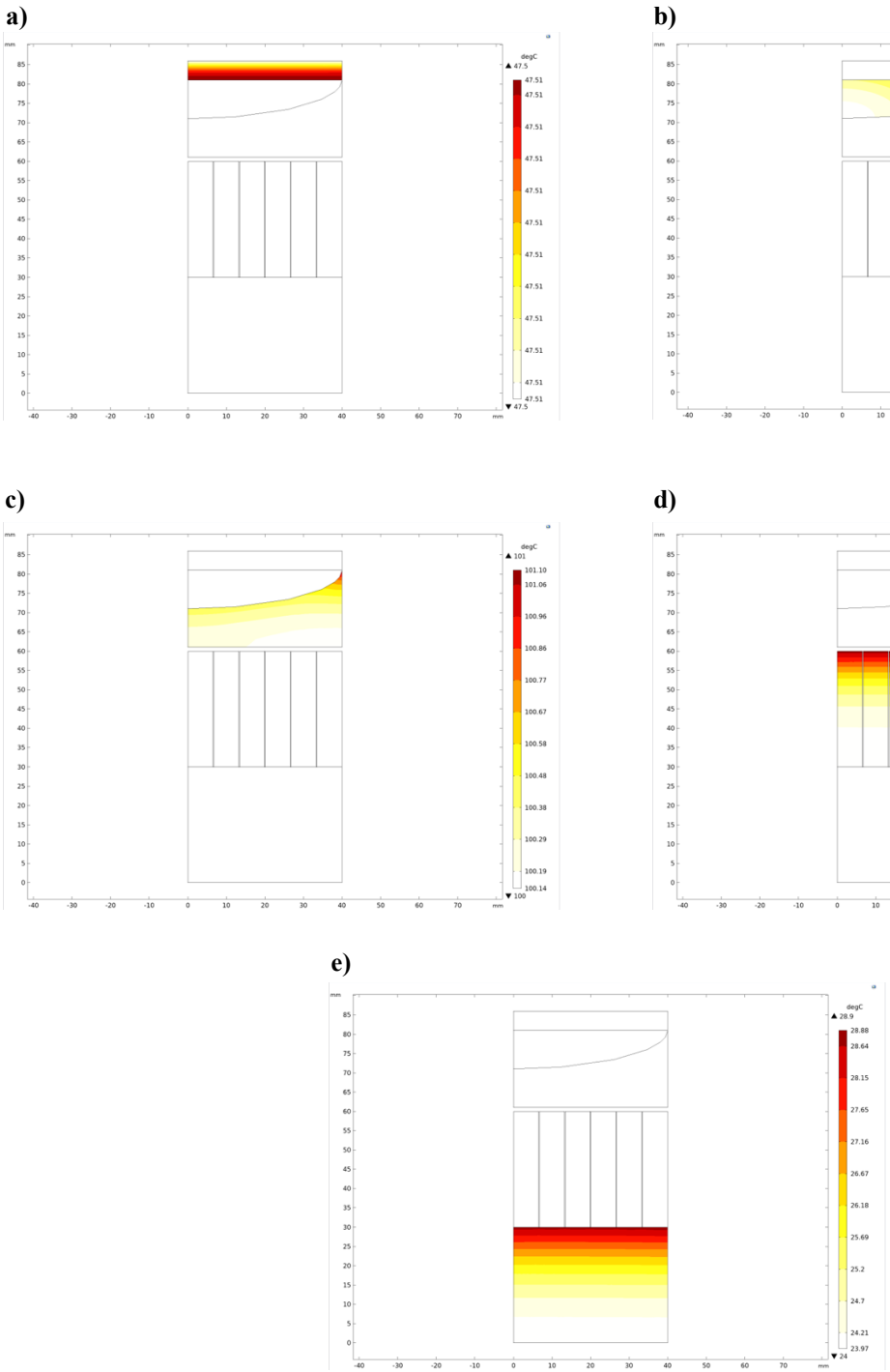

Figure 4-12 3D Temperature distribution of the evaporation system
Time = 3600 s

a) Transparent cover b) Spectrally selective solar absorber c) Copper porous foam
d) Air-laid paper e) Water bulk

a)

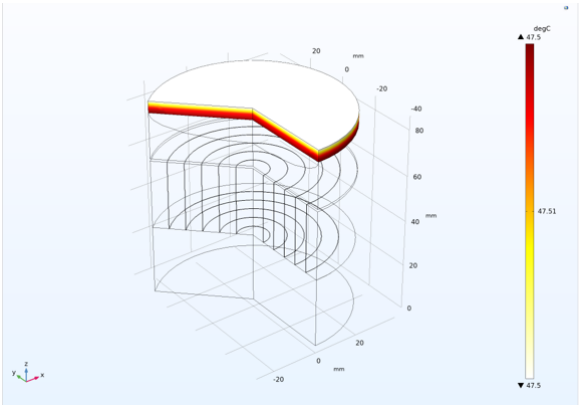

b)

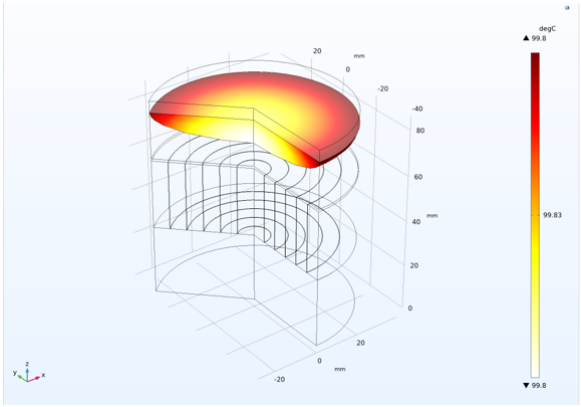

c)

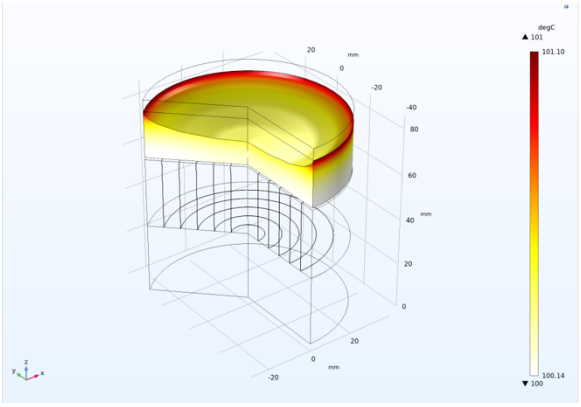

d)

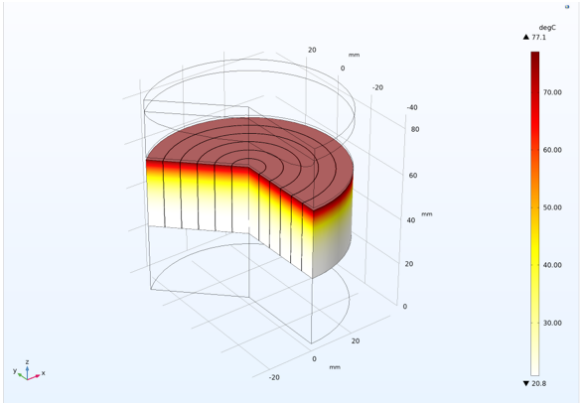

e)

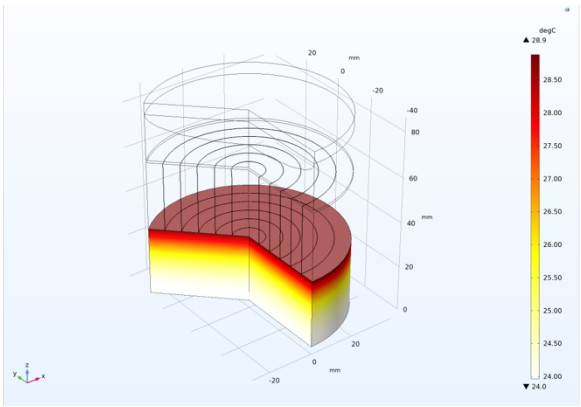

In addition, the influence of increased solar illumination intensity from 1, 3, 5, 7, 9, and 11-sun was investigated (Figure 4-13). The following figure shows that the more substantial solar flux shortens the heating-up time for the evaporator to achieve a steady state. For instance, when the solar flux is 5-sun, the design generates steam in 4 minutes. In addition, the heating-up time exhibits a fast decrease as the increased solar flux. Overall, the simulated trend and other experimental measured results are in good agreement. A marginally overestimated drop of the heating-up time by recreation might be due to the reality that the thermal contact resistance between each component inside the structure was not considered within the design.

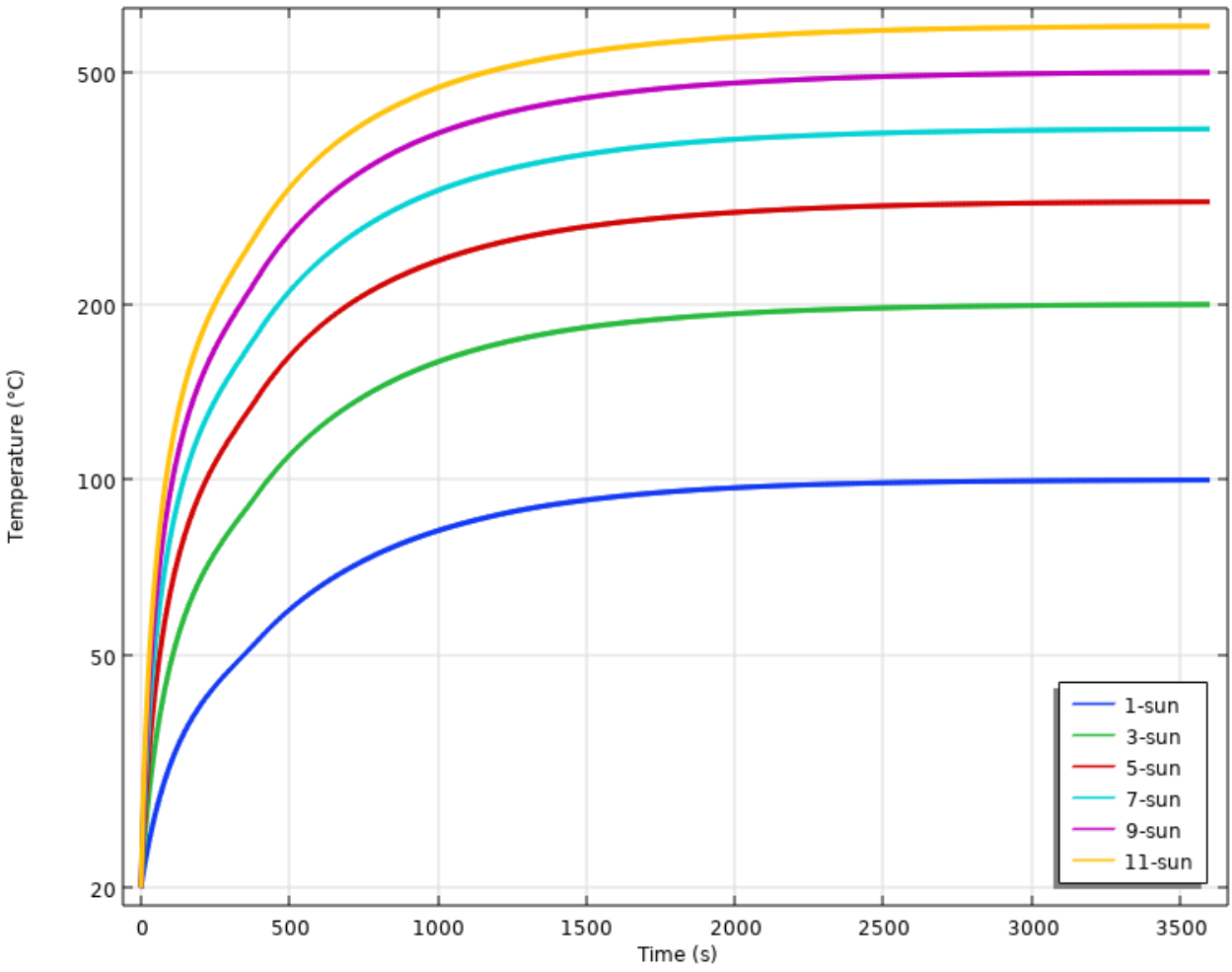

Figure 4-13 Evolution of steam temperature at different sun flux.

Chapter 5 Applications

Many technologically important energy-related applications have also been explored with the rapid development of solar-driven evaporation systems. Solar-driven interfacial evaporation can work specifically on open bodies of water without modern framework design, which would encourage its appropriation as a complementary innovation to concentrated solar power innovation for sun-based energy utilization and transformation at lower temperatures and pressures. Currently, the widely reported usages of solar-driven interfacial evaporation have been focused on:

- The Stem generation[24,27,49,51,53,54,73].
- Clean water generation through desalination[29,39,50,65].
- Water purification[57,59,75].

Concentrate solar-thermal heating in kept space, liquid-vapor stage alters, and quick heat and mass transport amid the interfacial evaporation handle offer extra means for changing over sun-powered energy into other shapes of energy[41,76-78]. Solar-driven interfacial evaporation has shown the capability to further promote the photocatalytic reaction due to increased temperature from solar-thermal heating and the accelerated diffusion of reactants driven by the vapor flow.

5.1 Solar-thermal energy harvesting and rapid transportation

To harvest solar energy, efficient solar-to-heat conversion and rapid transportation of the collected thermal energy with minimum loss to the application terminals are both critical. The hot vapor can serve as the carrier for quick delivery of the converted solar-thermal energy, as shown in Figure 5-1.

The generated heat instantly vaporized the underlying water, storing the solar-thermal energy within the hot vapors. The pressure difference drove the mists to quickly diffuse to the opposite cold end of the vacuum chamber and condense into liquid water, thereby releasing the carried latent heat to the external circulating water. Under capillary pumping from a hydrophilic wicking structure, the condensed water

spontaneously flowed back to the solar illumination and heat conversion region to complete the whole cycle. Such a device enables efficient transportation of a large capacity of solar-thermal energy with minimized heat loss due to the fast automatic cycling of evaporation and condensation processes. This interfacial dissipation plan has abbreviated the way of heat exchange, in this way decreasing the total thermal resistance of the gadget by more than 50%. The transparent window is the critical component that allows the transmission of solar light into the vacuum chamber to drive the interfacial evaporation. Still, its mechanical strength would limit the approach to moderate vapor pressures.

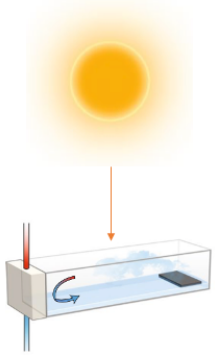

Figure 5-1 Floating solar absorber, within a sealed transparent vacuum chamber, placed at one end to convert the incident solar radiation into thermal energy. The fast liquid-to-vapour evaporation at the solar heating region and vapour-to-liquid condensation at the heat-releasing region enable efficient heat transfer of solar-thermal energy for heating applications far from the source of the heat.

5.2 Electricity generation

The dynamic flow of hot vapor, in particular high-pressure steam, can be directly applied to drive the rotation of gas turbines for power generation. Numerous of the detailed sun-powered-driven interfacial evaporation forms created low-temperature water vapor, but were incorrectly portrayed as water steam, which alludes to vapor over the bubbling temperature. Past sun-powered steam era at 100 °C beneath 1 atm through warm concentration[49], there are moreover investigations of producing high-temperature and high-pressure steam, which have stricter necessities on compelling water supply and physical strength of the evaporation framework.

Ambient solar-driven interfacial evaporation could also generate electricity. Recently, a team reported that an evaporation-induced salinity gradient could be harnessed to generate electricity[77] (Figure 5-2). The following figure appears to be a hybrid gadget composed of a solar-absorbing carbon-nanotube-modified paper film on top; an ion-selective layer on foot is floating at the air/seawater interface to receive solar radiation for concurrent solar desalination and electricity generation. The dissipation of water makes a saltiness angle from the dissipation surface to the bulk seawater, which drives the directional transport of salt ions. Under one sun illumination, the electrical power output density reached about 1 W m^{-2}, and the system has shown the potential to be scaled up.

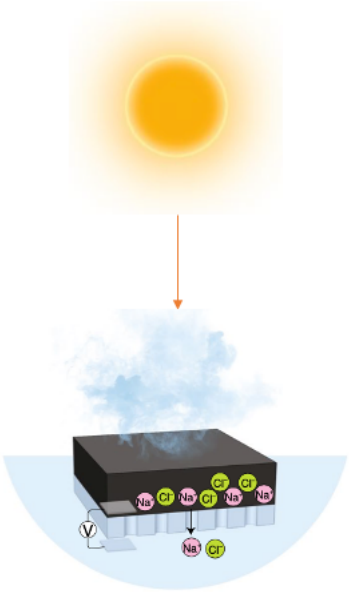

Figure 5-2 Schematic of evaporation-driven electricity generation. Solar-driven interfacial evaporation of slaty water creates the salinity gradient and the diffusion of sodium ions (pinks dots) across the membrane generates electricity.

However, it should be pointed out that the overall solar-to-electricity energy conversion efficiency from these processes is relatively low since most of the solar energy input has been used for water evaporation. The specialty application may be double-useful utilization of sun-oriented energy for both potable water and electrical power generation to drive low-power devices that function as sensors and other critical gadgets within the familiar environment.

5.3 Mechanical energy harvesting & Solar-chemical fuel production

The unique interfacial position and coupling of sun-oriented energy and vapor generation from the solar-driven interfacial evaporation produce the possibility of changing sun-based energy into mechanical and chemical fuels.

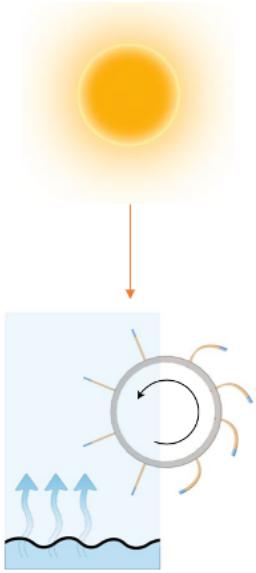

Figure 5-3 Schematic of mechanical energy harvesting. The strong bending–stretching response of the hydration-driven artificial muscle causes rotation of the moisture mill when it is exposed to the high humidity gradient created by the water evaporation.

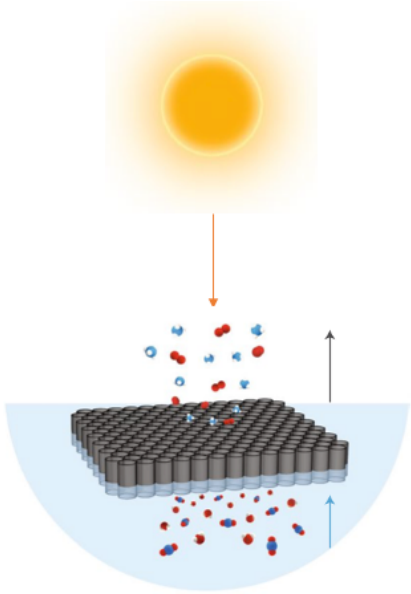

Figure 5-4 Schematic of flow-through solar-chemical fuels production. With the assistance of catalysts, carbon dioxide and water steam are converted into hydrocarbon fuels. The red, white and blue spheres represent oxygen, hydrogen and carbon atoms.

On the one hand, the changing humidity from the evaporated vapor at low temperatures (~30 °C) and normal pressure (1 atm) could induce mechanical motion in engines[77]. As appeared in Figure 5-3, a dampness process is situated at the air/water dissipating interface to make an expansive humidity difference. Half of the mill is within the humid environment where the films that are coated with moisture-sensitive spores are straightened, and the other half is exposed to the dry air in which the films bend. Such asymmetric bending shifts the mass center of the mill away and causes rotational motion, which could push a miniature car forward.

On the other hand, chemical fuels, in particular hydrogen, can be delivered through sun-powered thermochemical and photocatalytic processes in which hot water steam is blended with methane[79] or other biomasses[80] in a reactor often loaded with catalysts[78], as shown in Figure 5-4. In the steam–methanol reforming reaction, it has been found that the interfacial solar-thermal heating of the reaction solution that is wicked by a capillary to the liquid/air interface has higher hydrogen generation rates than the volumetric heating of the solution[79]. Interfacial warming can dodge the blockage of occurrence light by the produced gas bubbles the arrangement and has minor warm misfortunes to the ambient atmosphere.

Chapter 6 Conclusions

In summary, the porous solar-driven interfacial evaporator has been demonstrated to generate steam under low solar flux efficiently. The solar-to-steam conversion efficiency of the 3D porous solar-driven evaporation design is 48.1%. Managing the amount of water provided onto the porous evaporator surface is crucial to increasing the vapor temperature and anticipating overheating the evaporator, which minimizes heat misfortunes from the evaporation framework. The capillary pumping-based water supply permits us to innovate the surface wettability of the porous evaporator; therefore, adapting the water supply toward the evaporation region. The compact steam outlet design at the sidewall encourages the steam collection and resulting utilization of generated steam. With improved performance, porous interfacial evaporation can be used for solar-thermal energy harvesting and rapid transportation, electricity generation, mechanical energy harvesting, and solar-chemical fuel production. In addition, the generated steam as well can be directly used, for instance, in wax removal or be further pressurized to achieve even higher temperature for sterilization applications. I firmly believe that the high-efficiency portable steam generator is going to revolutionize the universal application of solar-thermal technologies under low solar flux since it has comprehensive accessibility of low-cost materials for manufacturing the evaporation framework and endlessly enables applications.

References

[1] Lewis, N. S. Research opportunities to advance solar energy utilization. Science, 2016, 351, 353.

[2] Crabtree, G. W. & Lewis, N. S. Solar energy conversion. Physics Today, 2007, 60, 37−42.

[3] Thirugnanasambandam, M.; Iniyan, S.; Goic, R. A review of solar thermal technologies. Renewable Sustainable Energy Reviews, 2010, 14, 312−322.

[4] Wang, Z.; Tong, Z.; Ye, Q.; et al. Dynamic tuning of optical absorbers for accelerated solar-thermal energy storage. Nature Communications, 2017, 8, 1478.

[5] Chu, S.; Cui, Y.; Liu, N. The path towards sustainable energy. Nature Materials, 2017, 16, 16–22.

[6] Weinstein, L. A; Loomis, J.; Bhatia, B.; et al. Concentrating solar power. Chemical Reviews, 2015, 115, 12797–12838.

[7] Kalogirou, S. A. Solar thermal collectors and applications. Progress in Energy and Combustion Science, 2004, 30, 231–295.

[8] Peng Tao; George Ni; Chengyi Song; et al. Solar-driven interfacial evaporation. Nature Energy, 2018, 3, 1031–1041.

[9] Roderick, M. L. & Farquhar, G. D. The cause of decreased pan evaporation over the past 50 years. Science, 2002, 298, 1410–1411.

[10] Ohmura, A. & Wild, M. Is the hydrological cycle accelerating? Science, 2002, 298, 1345–1346.

[11] Qiblawey, H. M. & Banat, F. Solar thermal desalination technologies. Desalination, 2008, 220, 633–644.

[12] Mills, D. Advances in solar thermal electricity technology. Solar Energy, 2004, 76, 19–31.

[13] Neumann, O.; Feronti, C.; Neumann, A. D.; et al. Compact solar autoclave based on steam generation using broadband light-harvesting nanoparticles. Proceedings of the National Academy of Science of the United States of America, 2013, 110, 11677−11681.

[14] Argiriou, A.; Klitsikas, N.; Balaras, C. A.; et al. Active solar space heating of residential buildings in northern Hellas-a case study. Energy and Building, 1997, 26, 215−222.

[15] Li, C.; Goswami, Y.; Stefanakos, E. Solar assisted sea water desalination: A review. Renewable and Sustainable Energy Reviews, 2013, 19, 136−163.

[16] Zhang, Y.; Zhao, D.; Yu, F.; et al. Floating rGO-based black membranes for solar driven sterilization. Nanoscale, 2017, 9, 19384−19389.

[17] Li, J.; Du, M.; Lv, G.; et al. Interfacial solar steam generation enables fast-responsive, energy-efficient, and low-cost off-grid sterilization. Advanced Materials, 2018, 1805159.

[18] Neumann, O.; Neumann, A. D.; Silva, E.; et al. Nanoparticle-mediated, light-induced phase separations. Nano Letters, 2015, 15, 7880−7885.

[19] Tiwari, G. N.; Singh, H. N.; Tripathi, R. Present status of solar distillation. Solar Energy, 2003, 75, 367−373.

[20] Chao Chang; Peng Tao; Benwei Fu; et al. Three-dimensional porous solar-driven interfacial evaporator for high-efficiency steam generation under low solar flux. ACS Omega, 2019, 4, 3546−3555.

[21] Osborne, N. S.; Stimson, H. F.; Ginnings, D. C. Measurements of heat capacity and heat of vaporization of water in the range 0 °C to 100 °C. Research of the National Institute of Standards and Technology, 1939, 23, 197−260.

[22] Shang, W. & Deng, T. Solar steam generation: Steam by thermal concentration. Nature Energy, 2016, 1, 16133.

[23] Wang, Z.; Liu, Y.; Tao, P.; et al. Bio-inspired evaporation through plasmonic film of nanoparticles at the air-water interface. Small, 2014, 10, 3234−3239.

[24] Ghasemi, H.; Ni, G.; Marconnet, A. M.; et al. Solar steam generation by heat localization. Nature Communications, 2014, 5, 4449. This scientific paper is one of the first introducing the concept of localized evaporation at the air/water interface for steam generation.

[25] Brongersma, M. L.; Halas, N. J.; Nordlander, P. Plasmon-induced hot carrier science and technology. Nature Nanotechnology, 2015, 10, 25.

[26] Zhang, L.; Tang, B.; Wu, J.; et al. Hydrophobic light-to-heat conversion membranes with self-healing ability for interfacial solar heating. Advanced Materials, 2015, 27, 4889−4894.

[27] Bae, K.; Kang, G.; Cho, S. K.; et al. Flexible thin-film black gold membranes with ultrabroadband plasmonic nanofocusing for efficient solar vapour generation. Nature Communications, 2015, 6, 10103.

[28] Wang, M.; Shan, J.; Chen, Z.; et al. Hierarchical graphene foam for efficient omnidirectional solar-thermal energy conversion. Advanced Materials, 2017, 29, 1702590.

[29] Li, X.; Xu, W.; Tang, M.; et al. Graphene oxide-based efficient and scalable solar desalination under one sun with a confined 2D water path. Proceedings of the National Academy of Science of the United States of America, 2016, 113, 13953−13958.

[30] Wang, Z. Z.; Ye, Q. X.; Liang, X. B.; et al. Paper-based membranes on silicone floaters for efficient and fast solar-driven interfacial evaporation under one sun. Journal of Material Chemistry A, 2017, 5, 16359−16368.

[31] Yang, Y.; Zhao, H.; Yin, Z.; et al. A general salt-resistant hydrophilic/ hydrophobic nanoporous double layer design for efficient and stable solar water evaporation distillation. Materials Horizons, 2018, 5, 1143−1150.

[32] Zhao, J.; Yang, Y.; Yang, C.; et al. A hydrophobic surface enabled salt-blocking 2D Ti_3C_2 MXene membrane for efficient and stable solar desalination. Journal of Material Chemistry A, 2018, 6, 16196−16204.

[33] Xu, N.; Hu, X.; Xu, W.; et al. Mushrooms as efficient solar steam-generation devices. Advanced Materials, 2017, 29, 1606762.

[34] Liu, H.; Chen, C.; Chen, G.; et al. High-performance solar steam device with layered channels: Artificial tree with a reversed design. Advanced Energy Materials, 2018, 8, 1701616.

[35] Chen, C.; Li, Y.; Song, J.; et al. Highly flexible and efficient solar steam generation device. Advanced Materials, 2017, 29, 1701756.

[36] Zhu, M.; Li, Y.; Chen, F.; et al. Plasmonic wood for high-efficiency solar steam generation. Advanced Energy Materials, 2017, 8, 1701028.

[37] Zhou, X.; Zhao, F.; Guo, Y.; et al. A hydrogel-based antifouling solar evaporator for highly efficient water desalination. Energy & Environmental Science, 2018, 11, 1985−1992.

[38] Liu, Y.; Yu, S.; Feng, R.; et al. A bioinspired, reusable, paper-based system for high-performance large-scale evaporation. Advanced Materials, 2015, 27, 2768−2774.

[39] Zhou, L.; Tan, Y.; Wang, J.; et al. 3D Self-assembly of aluminium nanoparticles for plasmon-enhanced solar desalination. Nature Photonics, 2016, 10, 393.

[40] Xu, W.; Hu, X.; Zhuang, S.; et al. Flexible and salt resistant janus absorbers by electrospinning for stable and efficient solar desalination. Advanced Energy Materials, 2018, 8, 1702884.

[41] Yang, P.; Liu, K.; Chen, Q.; et al. Solar-driven simultaneous steam production and electricity generation from salinity. Energy & Environmental Science, 2017, 10, 1923−1927.

[42] Zhu, L.; Gao, M.; Peh, C. K. N.; et al. Self-contained monolithic carbon sponges for solar-driven interfacial water evaporation distillation and electricity generation. Advanced Energy Materials, 2018, 8, 1702149.

[43] Li, Y.; Gao, T.; Yang, Z.; et al. 3D-Printed, all-in-one evaporator for high-efficiency solar steam generation under 1 sun illumination. Advanced Materials, 2017, 29, 1700981.

[44] Liu, Z.; Song, H.; Ji, D.; et al. Extremely cost-effective and efficient solar vapor generation under nonconcentrated illumination using thermally isolated black paper. Global Challenges, 2017, 1, 1600003.

[45] Ni, G.; Zandavi, S. H.; Javid, S. M.; et al. A salt-rejecting floating solar still for low-cost desalination. Energy & Environmental Science, 2018, 11, 1510−1519.

[46] Sajadi, S. M.; Farokhnia, N.; Irajizad, P.; et al. Flexible artificially networked structure for ambient/high pressure solar steam generation. Journal of Materials Chemistry A, 2016, 4, 4700− 4705.

[47] Jiang, Q.; Tian, L.; Liu, K. K.; et al. Bilayered biofoam for highly efficient solar steam generation. Advanced Material, 2016, 28, 9400−9407.

[48] Cooper, T. A.; Zandavi, S. H.; Ni, G. W.; et al. Contactless steam generation and superheating under one sun illumination. Nature Communications, 2018, 9, 5086.

[49] Ni, G.; Li, G.; Boriskina, S. V.; et al. Steam generation under one sun enabled by a floating structure with thermal concentration. Nature Energy, 2016, 1, 16126. This work systematically analyses the energy balance for solar-driven interfacial evaporation systems, and demonstrates the thermal concentration strategy to generate steam with the solar-driven interfacial evaporator under a low solar flux level.

[50] Zeng, Y.; Yao, J.; Wang, K.; et al. Solar evaporation enhancement using floating light-absorbing magnetic particles. Energy & Environmental Science, 2011, 4, 4074–4078.

[51] Ito, Y.; Tanabe, Y.; Han, J.; et al. Multifunctional porous graphene for high-efficiency steam generation by heat localization. Advanced Materials, 2015, 27, 4302–4307.

[52] Hu, X. Z.; Xu, W.; Tan, Y.; et al. Tailoring graphene oxide-based aerogels for efficient solar steam generation under one sun. Advanced Materials, 2016, 29, 1604031.

[53] Zhou, L.; Ji, D.; Zhang, P.; et al. Self-assembly of highly efficient, broadband plasmonic absorbers for solar steam generation. Science Advances, 2016, 2, e1501227.

[54] Wang, X.; He, Y.; Liu, X.; et al. Solar steam generation through bio-inspired interface heating of broadband-absorbing plasmonic membranes. Applied Energy, 2017, 195, 414–425.

[55] Kuzmenko, A. B.; Van Heumen, E.; Carbone, F.; et al. Universal optical conductance of graphite. Physical Review Letters, 2008, 100, 117401.

[56] Xue, G.; Liu, K.; Chen, Q.; et al. Robust and low-cost flame-treated wood for high-performance solar steam generation. ACS Applied Materials & Interfaces, 2017, 9, 15052–15057.

[57] Ma, S.; Zhu, Y.; Long, H.; et al. Recycled waste black polyurethane sponges for solar vapor generation and distillation. Applied Energy, 2017, 206, 63–69.

[58] Wang, G.; Fu. Y.; Guo, A.; et al. Reduced graphene oxide-polyurethane nanocomposite foams as a reusable photo-receiver for efficient solar steam generation. Chemistry of Materials, 2017, 29, 5629–5935.

[59] Lou, J.; Liu, Y.; Wang, Z.; et al. Bioinspired multifunctional paper-based RGO composites for solar-driven clean water generation. ACS Applied Materials & Interfaces, 2016, 8, 14628–14636.

[60] Richardson, H.; Carlson, T.; Tandler, J.; et al. Experimental and theoretical studies of light-to-heat conversion and collective heating effects in metal nanoparticle solutions. Nano Letters, 2009, 9, 1139–1146.

[61] Neumann, O.; Urban, A.; Day, J.; et al. Solar vapor generation enabled by nanoparticles. ACS Nano, 2012, 7, 42–49.

[62] Jin, H.; Lin, G.; Bai, L.; et al. Steam generation in a nanoparticle-based solar receiver. Nano Energy, 2016, 28, 397–406.

[63] Hogan, N. J.; Urban, A. S.; Ayala-Orozco, C.; et al. Nanoparticles heat through light localization. Nano Letters, 2014, 14, 4640–4645.

[64] Deng, Z.; Zhou, J.; Lui, C.; et al. The emergence of solar thermal utilization: solar-driven steam generation. Journal of Materials Chemistry A, 2017, 5, 7691–7709.

[65] Liu, Y.; Yu, S.; Feng, R.; et al. A bioinspired, reusable, paper-based system for high-performance large-scale evaporation. Advanced Materials, 2015, 27, 2768−2774.

[66] Guler, U.; Shalaev, V. M.; Boltasseva, A. Nanoparticle plasmonics: Going practical with transition metal nitrides. Materials Today, 2015, 18, 227–237.

[67] Ishii, S.; Sugavaneshwar, R. P.; Nagao, T. Titanium nitride nanoparticles as plasmonic solar heat transducers. Journal of Physical Chemistry C, 2015**,** 120, 2343–2348.

[68] Cao, F.; McEnaney, K.; Chen, G.; et al. A review of cermet-based spectrally selective solar absorbers. Energy & Environmental Science, 2014, 7, 1615–1627.

[69] Zhao, D.; Duan, H.; Yu, S.; et al. Enhancing localized evaporation through separated light absorbing centers and scattering centers. Scientific Reports, 2015, 5, 17276.

[70] Wang, Z.; Liu, Y.; Tao, P.; et al. Bio-inspired evaporation through plasmonic film of nanoparticles at the air-water interface. Small, 2014, 10, 3234−3239.

[71] Liu, Y.; Chen, J.; Guo, D.; et al. Floatable, self-cleaning, and carbon-black-based superhydrophobic gauze for the solar evaporation enhancement at the air–water interface. ACS Applied Materials & Interfaces, 2015, 7, 13645–13652.

[72] Yu, S.; Zhang, Y.; Duan, H.; et al. The impact of surface chemistry on the performance of localized solar-driven evaporation system. Scientific Reports, 2015, 5, 13600.

[73] Hu, X. Z.; Xu, W. C.; Tan, Y. L.; et al. Tailoring graphene oxide-based aerogels for efficient solar steam generation under one sun. Advanced Materials, 2016, 29, 1604031.

[74] Wang, Z.; Ye, Q. X.; Liang, X. B.; et al. Paper-based membrane on silicone floater for efficient and fast solar-driven interfacial evaporation under one sun. Journal of Materials Chemistry A, 2017, 5, 16359–16368.

[75] Dongare, P. D.; Alabastri, A.; Pedersen, S.; et al. Nanophotonics-enabled solar membrane distillation for off-grid water purification. Proceedings of the National Academy of Science of the United States of America, 2017, 114, 6936–6941.

[76] Chang, C.; Yang, C.; Liu, Y. M.; et al. Efficient solar-thermal energy harvest driven by interfacial plasmonic heating-assisted evaporation. ACS Applied Materials & Interfaces, 2016, 8, 23412–23418.

[77] Chen, X.; Goodnigh, D.; Gao, Z. H.; et al. Scaling up nanoscale water-driven energy conversion into evaporation-driven engines and generators. Nature Communications, 2014, 6, 7346.

[78] Varghese, O. K.; Paulose, M.; LaTempa, T. J.; et al. High-rate solar photocatalytic conversion of CO_2 and water vapor to hydrocarbon fuels. Nano Letters, 2009, 9, 731–737.

[79] Lee, M. T.; Werhahn, M.; Hwang, D. J.; et al. Hydrogen production with a solar steam-methanol reformer and colloid nanocatalyst. International Journal of Hydrogen Energy, 2010, 35, 118–126.

[80] Ravaghi-Ardebili, Z.; Manenti, F.; Corbetta, M.; et al. Biomass gasification using low-temperature solar-driven steam supply. Renewable Energy, 2015, 74, 671–680.

Acknowledgments

As time goes by, six years of college life, four years at Tianjin University, China, and two years at Pontifical Catholic University of Peru, Peru, will be over instantly. Looking back on the years, these years of college life, the arduous journey of study, accompanied and supported by teachers, friends and classmates, were terrific!

I would like to thank my supervisor, Mr. Xian Hua, for his rich professional knowledge and scientific research spirit greatly influence me. On top of that, I do appreciate that Mr. Xian Hua made time to guide me, cultivate my ideas, contribute many suggestions, put forward timely modification suggestions, and patiently review and revise my thesis. Every detail and data of this paper cannot be separated from his careful guidance.

I am thankful to the School of Environmental Science and Engineering, which gave me a lot of opportunities to exercise myself and provided many platforms to be myself. I would always be thankful for the people who have helped and cared for me during my bachelor's degree journey. I will bear in mind what you have done for me. Although my thoughts are very feeble at this moment while I am writing…, I do want to say, "Thank you, Tianjin University, professors, and all my friends from China!".

Sincerely,

Pierre Alexander Porras Jorge